Pergamon

Continental Shelf Research, Vol. 15, No. 13, pp. 1597–1630, 1995

0278–4343/95 $9.50 + 0.00

0278–4343(95)00034–8

Haline stratification in the Rhine–Meuse freshwater plume: a three-dimensional model sensitivity analysis

K. G. RUDDICK,* E. DELEERSNIJDER,† P. J. LUYTEN* and J. OZER*

(*Received* 2 *August* 1994; *accepted* 20 *March* 1995)

Abstract—Results are presented of a three-dimensional model study of the tidally-averaged salinity field in the Rhine–Meuse plume. In conditions of low mixing (no wind, neap tide) freshwater emerges from the river as a jet, turns right under the influence of Coriolis force and attaches to the coast as a buoyancy current. Surface residual currents are essentially geostrophic. Within the plume the surface layer is strongly stratified and overlies a bottom mixed layer.

Results are strongly sensitive to the parameterization of vertical mixing: models ranging from constant diffusion coefficients through simple algebraic Richardson number dependent formulations to turbulence closure with evolution equations for turbulent kinetic energy and length scale were tested. Turbulence closure with a single evolution equation for turbulent kinetic energy and an algebraic length scale formulation was found to provide a suitable balance between physical realism (assessed by theoretical considerations and the practical ability to represent a well-mixed bottom boundary layer and stratified surface layer) and computational efficiency. Simpler models, which vary diffusion coefficients as function of Richardson number, may produce similar results, though require more careful calibration. Constant diffusion coefficients are clearly inadequate for the application considered. Even the preferred "k" model requires some calibration as a "background" or "ambient" mixing coefficient had to be introduced to avoid unrealistically strong stratification.

The tidally-averaged salinity field was found to be qualitatively similar at neap and spring tide, though cross-shore penetration of the outflow jet was reduced, bottom-mixed layer thickness increased and overall stratification reduced at springs. In contrast, the salinity field was found to be strongly dependent on wind strength and direction, both through wind-induced surface mixing and advection by wind-driven surface currents.

1. INTRODUCTION

1.1. *Need for sensitivity analysis*

The main focus of this paper is an investigation of the sensitivity of the results of a three-dimensional model of the Rhine–Meuse freshwater plume to the parameterization of vertical mixing processes.

*Management Unit of Mathematical Models of the North Sea and Scheldt Estuary (MUMM), Gulledelle 100, B-1200 Brussels, Belgium.

†Institut d'Astronomie et de Géophysique G. Lemaître, Université Catholique de Louvain, Chemin du Cyclotron 2, B-1348 Louvain-la-Neuve, Belgium.

Three-dimensional models are frequently used to simulate shelf sea hydrodynamics (e.g. Heaps, 1987; Nihoul and Jamart, 1987), and the results of such models are compared with selected measurements to demonstrate "validity" of the model or to elucidate poorly understood phenomena. However, the procedure of representing a physical system by a mathematical model, and then discretizing and programming that model introduces discrepancies between the physical system (or, more precisely, measurements of the physical system) and the output of the computer program. A potentially important source of such discrepancy is the parameterization of sub-grid scale effects by diffusion coefficients, particularly in regions of strong haline or thermal stratification, where there is considerable spatial and temporal variability in turbulent diffusion. According to the state-of-the-art review of coastal modelling by the "Group of Experts on the Scientific Aspects of Marine Pollution" GESAMP (1991):

> "(p. 36) Many of the processes that influence the magnitude of the diffusion coefficients for contaminants, salinity, temperature and momentum (eddy viscosity) are poorly known. However, these processes significantly influence the dispersion of the contaminant and the associated flow field".
>
> "(p. 110) A range of formulations/parameterizations of these mixing processes must be considered. If such a sensitivity study shows that contaminant distributions are sensitive to the formulation of mixing parameters (this is usually the case), then a confidence limit can be placed on the model based upon the accepted range of parameterizations of the mixing process. In the unlikely event that a sensitivity analysis reveals that the model is insensitive to the formulation of mixing, then only the simplest formulation of the process is required".

Therefore, in order to assess the confidence that can be placed on simulations of the dispersion of freshwater from a river discharge and to provide recommendations on the level of complexity required in parameterizing vertical diffusion processes, such a sensitivity study has been undertaken here for a range of popular turbulence models.

Obviously statements of sensitivity to parameterization depend on the item/process of interest. Here, the tidally-averaged "residual" salinity field has been chosen as the model output for which sensitivity is to be analysed. The salinity distribution is of interest both because of its influence on currents [via eddy viscosity, e.g. Visser *et al.* (1994) and density-induced pressure gradients, e.g. Heaps (1972)], and more generally as a tracer for other dissolved substances. Conclusions relating to the dispersion of freshwater are applicable to any conserved scalar discharged with freshwater, including dissolved substances of ecological interest. Indeed, the suitability of salinity as a tracer is exploited by Laane *et al.* (1989) to efficiently monitor long-term changes in inorganic phosphorus and nitrogen in the Dutch coastal zone—the salinity–nitrate correlation in winter can be used to remove short time variability.

1.2. *Physical oceanography of the Rhine plume region*

Campaigns by Dutch scientists over the last decade have enabled aspects of the salinity distribution in the Dutch coastal zone to be described. Measurements by van Alphen *et al.* (1988) averaged over 20 campaigns in 1985 show that haline stratification extends at least 10 km and up to 100 km from the mouth of the Rhine. Salinity fields averaged over eight cruises in 1986 and 1987 are described by de Ruijter *et al.* (1992) showing a Northeastward

residual drift of freshwater from the Rhine–Meuse discharge. Clearly considerable mesoscale variability has been averaged out of such measurements. The factors determining to a large extent hydrography in the Dutch coastal zone are the tide, wind and river discharge.

1.2.1. *Tide*. As for much of the Southern Bight of the North Sea, the energy spectrum is dominated by semi-diurnal tidal variability (Zimmerman, 1986), in particular the M_2 component, which induces depth-mean currents of about 0.6 m s^{-1} (Bos *et al.*, 1991). The second largest tidal component, S_2 (with associated depth-mean currents of about 0.15 m s^{-1}), beats with the M_2 component to give a semi-diurnal signal modulated over the spring–neap cycle. Vertically sheared cross-shore and along-shore tidal currents generate significant semi-diurnal variability of stratification (Simpson and Souza, 1995). The role of the barotropic tidal residual is less clear, though seems small compared to wind and density-driven residuals—computations by Gerritsen (1983) using a depth-integrated model suggest a barotropic tidal residual of about 0.03 m s^{-1}. Horizontal dispersion by tidal horizontal advection and vertical diffusion is highly anisotropic—de Kok (1994) reports along-shore dispersion coefficients an order of magnitude higher than cross-shore dispersion coefficients.

1.2.2. *Wind*. Three-dimensional residual current structure, and hence salinity, is rather sensitive to wind. Van der Giessen *et al.* (1990) describe residual currents 10 km offshore of Noordwijk for winds from four different sectors, and show that wind-induced residual currents are significant compared to density-induced along-shore geostrophic and cross-shore "estuarine" residual currents. Analysis of current measurements made 10 km offshore of the river mouth by Gerritsen and Scholten (1985) show meteorologically driven residual currents of up to 0.15 m s^{-1} for wind speeds of about 8 m s^{-1}. Simpson *et al.* (1993) show that in well-mixed conditions the bottom and surface along-shore residual currents are strongly correlated and the whole water column responds to wind, while for stratified conditions the bottom and surface layers are only weakly coupled—cross-shore currents respond less strongly to wind because of set-up against the coastal boundary.

"Straining" (vertically-sheared horizontal advection) of the salinity field by wind-driven cross-shore circulation contributes significantly to stratification dynamics with onshore surface currents tending to destroy stratification and offshore surface currents increasing stratification by advecting freshwater offshore to tens of kilometres (de Ruijter *et al.*, 1992). Wind also influences the salinity field by enhancing turbulent mixing and, thus, tending to reduce stratification.

1.2.3. *River discharge*. Mesoscale variability of the river discharge is dominated by semi-diurnal tidal flushing of the estuary, which may result in distinct patches of freshwater originating from different low tides as depicted by van Alphen *et al.* (1988).

2. METHOD

2.1. *Governing equations for shallow sea hydrodynamics*

The governing equations for shallow sea hydrodynamics are obtained from considering conservation of mass, momentum and salinity using the Boussinesq approximation, the

Table. 1. Physical parameters used in simulations and empirical constants for the turbulence model (Mellor and Yamada, 1982)

Coriolis frequency f	$1.146 * 10^{-4}\ \mathrm{s}^{-1}$
Gravitational acc. g	$9.81\ \mathrm{m\ s}^{-2}$
Reference density ρ_0	$1027.4\ \mathrm{kg\ m}^{-3}$
Reference salinity S_0	34.5 psu
Haline expansivity β_S	$0.766 * 10^{-3}\ \mathrm{psu}^{-1}$
Roughness length z_0	$6.0 * 10^{-3}\ \mathrm{m}$
Empirical constant A_1	0.92
Empirical constant A_2	0.74
Empirical constant B_1	16.6
Empirical constant B_2	10.1
Empirical constant C_1	0.08
Empirical constant E_1	1.8
Empirical constant E_2	1.33

boundary layer approximation (including hydrostatic equilibrium) and the representation of unresolved turbulent fluctuations by an eddy viscosity and diffusivity, ν_T and λ_T. The state variables employed are horizontal velocity, $\mathbf{u}$, vertical velocity, w, practical salinity, S, and reduced pressure, q, and are given for the Cartesian coordinate system, (x,y,z), with horizontal unit vectors $\mathbf{e}_x,\mathbf{e}_y$ and vertical (upwards) unit vector $\mathbf{e}_z$. q is defined by

$$q = \frac{P - P_{\mathrm{atm},0}}{\rho_0} + gz \tag{1}$$

where P is the pressure, $P_{\mathrm{atm},0}$ is a reference atmospheric pressure, ρ_0 is a reference density and g is the gravitational acceleration. The buoyancy, b, relative to a reference salinity, S_0, is obtained by considering a linearized equation of state, neglecting the effect of temperature variations on density, which is dominated by salinity variation for this region,

$$b = \beta_{Sg}(S_0 - S) \tag{2}$$

where β_S is the coefficient of haline expansivity. The numerical values for the various constants are given in Table 1. Evolution of the state variables is given by:

$$\nabla_h \cdot \mathbf{u} + \frac{\partial w}{\partial z} = 0 \tag{3}$$

$$\frac{\partial q}{\partial z} = b \tag{4}$$

$$\frac{\partial \mathbf{u}}{\partial t} + \nabla_h \cdot (\mathbf{uu}) + \frac{\partial (w\mathbf{u})}{\partial z} - \frac{\partial}{\partial z}\left(\nu_T \frac{\partial \mathbf{u}}{\partial z}\right) = -f\mathbf{e}_z \otimes \mathbf{u} - \nabla_h q \tag{5}$$

$$\frac{\partial S}{\partial t} + \nabla_h \cdot (\mathbf{u}S) + \frac{\partial (wS)}{\partial z} - \frac{\partial}{\partial z}\left(\lambda_T \frac{\partial S}{\partial z}\right) = 0 \tag{6}$$

where f is the Coriolis frequency and the horizontal gradient operator is given by,

$$\nabla_h = \mathbf{e}_x \frac{\partial}{\partial x} + \mathbf{e}_y \frac{\partial}{\partial y}. \tag{7}$$

Horizontal diffusion is often used in large (super-meso) scale models to represent processes which cannot be resolved by the grid size and/or time step employed. However, in the present study the grid is small enough (1 km) to represent, for example, features with the size of the baroclinic Rossby radius (~4 km), and the time step is small enough (300 s) to capture the dominant tidal processes; since a typical transit time for freshwater to be advected from the river mouth to a boundary of the domain is estimated as $t_a \sim 5 * 10^5$s, a horizontal diffusion coefficient, $A_h \sim 2\ \mathrm{m^2\ s^{-1}}$, typical of that suggested by dye diffusion experiments (Okubo, 1971), would only affect features with horizontal length scales $< \sqrt{A_h t_a} \sim 1$ km, which is not larger than the grid size. Horizontal diffusion is, therefore, not required to represent physical processes [nor is horizontal diffusion necessary or desirable for numerical reasons, e.g. Deleersnijder and Wolanski (1990), since the advection scheme is designed to be numerically stable and to supply sufficient diffusion for nearly monotonic solutions]. Unresolved mixing processes are, thus, represented only as vertical diffusion.

2.2. *Numerical discretization*

The model MU-ROFI has been developed to solve the governing equations (3)–(6). The choice of numerical methods [finite differences, Arakawa C grid, sigma transformation, explicit horizontal and implicit vertical derivatives in (5) and (6), mode-splitting, etc.] follows closely the work of Blumberg and Mellor (1987), Beckers (1991) and Deleersnijder (1992). Preliminary application of this model to study semi-diurnal front formation and downwelling in the Rhine discharge zone is described by Ruddick *et al.* (1994). Model improvements made since that study include a hierarchy of turbulence closure models (described in Section 2.4) and a hybrid advection scheme based on the work of James (1986)—this gives a second-order scheme in regions of smooth salinity variation and a first-order, monotonic scheme near fronts.

2.3. *Grid*

Simulations were performed for the Rhine plume region indicated in Fig. 1, and using the grid and bathymetry shown in Fig. 2. A horizontal grid with dimensions $L_x = 80$ km by $L_y = 40$ km was used with grid spacing, $\Delta x = \Delta y = 1$ km and 20 σ-layers. A time step of $\Delta t_{2D} = 30$ s was used for the external, depth-integrated mode (within the stability criterion) and $\Delta t_{3D} = 300$ s was used for the internal mode.

2.4. *Parameterization of sub-grid scale effects*

In the derivation of (5), (6) it has been assumed that the mixing arising from processes which cannot be resolved by the numerical grid, can be represented by turbulent or "eddy" viscosity and diffusion coefficients, ν_T and λ_T. It is supposed that influence from small to large scales is primarily through the mixing achieved by three-dimensional turbulent fluctuations.

The mathematical description of turbulence is a major unsolved problem of modern physics, and is the subject of considerable research activity. Moreover, geophysical

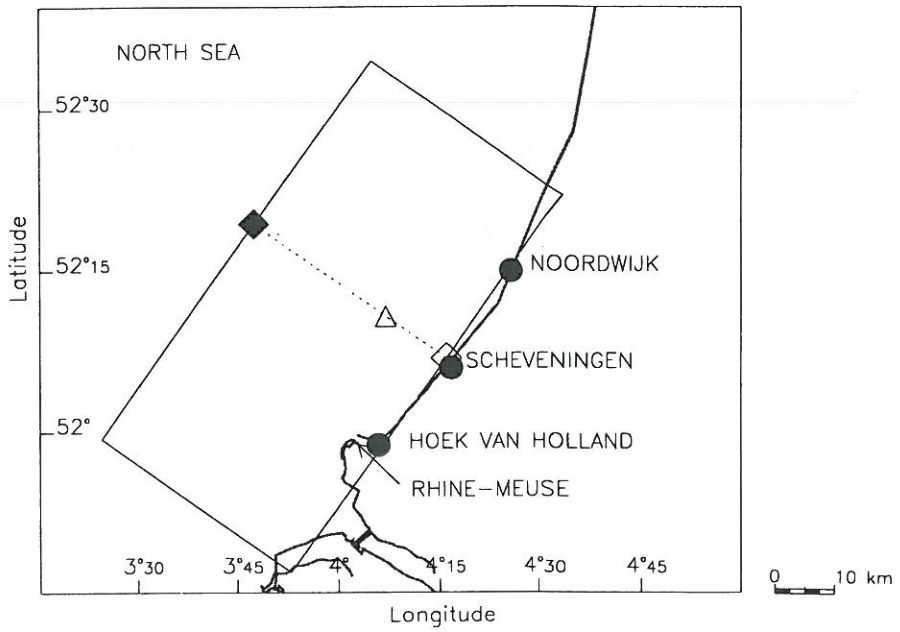

Fig. 1. The domain of interest showing the location of the grid, the cross-shore transect ◇ ↔ ◆ and the "mooring" △ used for the presentation of results.

turbulence is complicated by stratification. Overviews of geophysical turbulence modelling can be found in Nihoul (1980), Rodi (1984) and Mellor (1985). Attention here will be restricted to the application of turbulence closure models used in practical geophysical calculations, ranging from simple, constant diffusion coefficients, through algebraic Richardson-number dependent formulations to models with evolution equations for turbulent kinetic energy density, k, and turbulence macro length scale, l (or a suitable product of k and l).

2.4.1. *Quasi-equilibrium Mellor–Yamada–Galperin level* 2.5 k-kl *model ("k–kl" Model)*. The most complex model to be considered here requires the solution of evolution equations for k and kl, as designed by Mellor and Yamada (1974, 1982). Advection of turbulent quantities is not considered here, since, while not always negligible in comparison to production and destruction terms, for many applications inclusion of advection of turbulence introduces considerable practical problems (grid staggering, lateral boundary condition), which are difficult to justify in terms of more realistic results—a justification for the neglection of advection of turbulence in stratified regions is given in Appendix B. The time evolution of k and kl is given in (8) and (9), where the right-hand side terms represent production of turbulence by shear of the mean flow, exchange between turbulent kinetic energy and potential energy, viscous dissipation and vertical diffusion, respectively.

$$\frac{\partial k}{\partial t} = l\sqrt{2k}\, S_u M^2 - l\sqrt{2k}\, S_b N^2 - \frac{2^{3/2}k^{3/2}}{B_1 l} + \frac{\partial}{\partial z}\left(\lambda_T^k \frac{\partial k}{\partial z}\right) \tag{8}$$

$$\frac{\partial kl}{\partial t} = \frac{E_1 l}{2} l\sqrt{2k}\, S_u M^2 - \frac{E_1 l}{2} l\sqrt{2k}\, S_b N^2 - \frac{W2^{1/2}k^{3/2}}{B_1} + \frac{\partial}{\partial z}\left(\lambda_T^k \frac{\partial kl}{\partial z}\right) \tag{9}$$

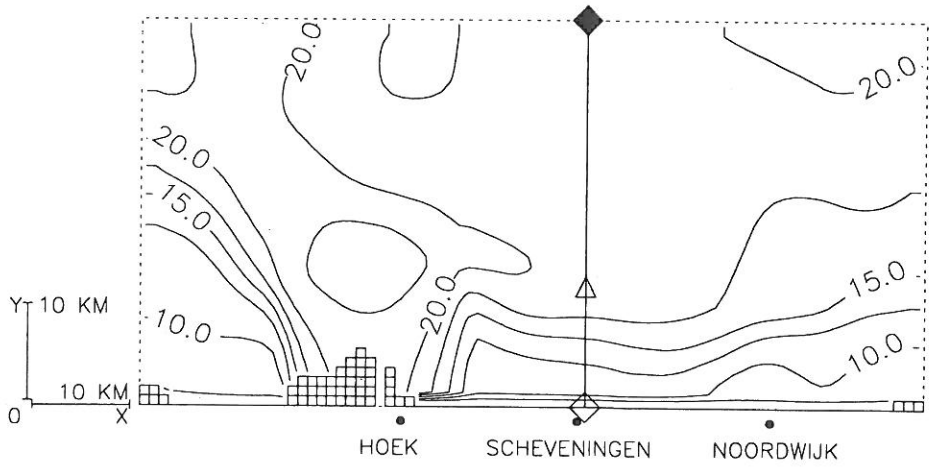

Fig. 2. The bathymetry of the computational grid and the cross-shore transect ◇ ⟷ ◆ and the "mooring" △ used for the presentation of results.

where the shear frequency, M, and Brunt–Väisala frequency, N, are given by

$$M^2 = \left(\frac{\partial u}{\partial z}\right)^2 + \left(\frac{\partial v}{\partial z}\right)^2 \tag{10}$$

$$N^2 = \frac{\partial b}{\partial z} \tag{11}$$

and the "wall proximity function" W by

$$W = 1 + E_2\left(\frac{lH}{\kappa d_s d_b}\right)^2 \tag{12}$$

where $d_s = \eta - z$ and $d_b = z + h$ are the distance from the sea surface ($z = +\eta$) and the sea bottom ($z = -h$), $\kappa = 0.40$ is the von Karman constant, and $H = h + \eta$ is the total water depth.

The turbulent diffusion coefficients needed in (5), (6), (8), (9) are given by

$$(\nu_T, \lambda_T, \lambda_T^k) = l\sqrt{2k}\,(S_u, S_b, S_k) \tag{13}$$

where the stability functions are given by Galperin *et al.* (1988) as

$$S_u = A_1 \frac{1 - 3C_1 - 6\dfrac{A_1}{B_1} - 3A_2G\left[(B_2 - 3A_2)\left(1 - 6\dfrac{A_1}{B_1}\right) - 3C_1(6A_1 + B_2)\right]}{[1 - 3A_2G(6A_1 + B_2)](1 - 9A_1A_2G)} \tag{14}$$

$$S_b = A_2 \frac{1 - 6\dfrac{A_1}{B_1}}{1 - 3A_2G(6A_1 + B_2)} \tag{15}$$

$$S_k = 0.2 \tag{16}$$

where

$$G = -\frac{N^2 l^2}{2k}. \tag{17}$$

The empirical constants, calibrated from laboratory experiments, are given in Table 1. This formulation of the stability functions have been shown by Deleersnijder and Luyten (1994) to be numerically more robust than the original formulation by Mellor and Yamada (1982).

The theoretical basis for this turbulence closure model, and probably for all others, is generally regarded to be weak for strongly stratified flows, where turbulence ceases and $k \to 0$, $l \to 0$. This is the subject of considerable research activity, e.g. Hopfinger (1987). The approach adopted here, following Galperin *et al.* (1988) is to limit l by appealing to experimental studies of stably stratified flows, which suggest limitation of the size of turbulent eddies by stable stratification. Accordingly,

$$l \leqslant \sqrt{\frac{0.56k}{\max(0, N^2)}} \tag{18}$$

$$G \geqslant -0.28. \tag{19}$$

A further condition

$$G \leqslant 0.023 \tag{20}$$

is applied to G in the case of unstable stratification to ensure that an equilibrium solution to (8) is possible, thus preventing k from growing unboundedly.

Such a turbulence closure gives strong suppression of turbulence in stratified regions, where turbulent diffusion coefficients decrease to their molecular values. While this is physically realistic for laboratory conditions, the assumption that all sub-grid scale mixing for a three-dimensional marine model can be parameterized as three-dimensional turbulence is dubious. Thus, in the absence of wind and above the tidally-mixed bottom layer, if molecular diffusion is the only mixing process the length scale over which spreading surface freshwater mixes with underlying ambient water could be thousands of kilometres (a simple dimensional analysis is presented in Appendix A). Yet measurements of the salinity field in the Rhine plume indicate that, even in extreme conditions of low wind, considerable mixing takes place, suggesting that vertical mixing is indeed stronger than just molecular diffusion. Thus, in all models considered here the diffusion coefficients are limited

$$[\nu_T, \lambda_T, \lambda_T^k] = l\sqrt{2k}\,[S_u, S_b, S_k] + \lambda_{\min} \tag{21}$$

by a minimal or "background" or "ambient" mixing coefficient, $\lambda_{\min}$, which is intended to represent all other forms of unresolved mixing. The need for an arbitrarily assigned background coefficient was also found by e.g. Martin (1985) and Sharples and Simpson (1995), though must be considered as an important deficiency in current theories of mixing in strongly stratified marine flows.

2.4.2. *Quasi-equilibrium Mellor–Yamada–Galperin level* 2.5 k *model* ("k" *Model*). Since it is generally recognized, e.g. Mellor and Yamada (1982), Rodi (1984), Nihoul *et al.*

(1989), that the evolution equation for kl is the weak point of the above model, it is common to replace (9) by a simpler algebraic equation for l, thus reducing computational complexity and expense. For example, a simple parabolic vertical profile

$$l = \frac{\kappa d_b d_s}{H} \tag{22}$$

is considered here. This formulation gives the desired asymptotic behaviour, $l \sim \kappa d_b$ in neutrally stratified conditions in the bottom boundary layer, and still accounts for reduction of l in stratified regions via the limitation (18).

2.4.3. *Equilibrium Mellor–Yamada–Galperin level 2 model ("level 2" model).* Equation (8) can be simplified to an algebraic equation by assuming that vertical diffusion of k can be neglected and that adjustment of k to turbulent equilibrium is rapid (i.e. $\partial k/\partial t$ can be neglected).

This yields a quadratic equation for k/l^2, e.g. Davies *et al.* (1995), [the limitations (18,19) on G are not applied in the level 2 model] which can be solved to give an algebraic equation

$$[\nu_T, \lambda_T] = l^2 M[F^{\nu}_{L2}(Ri), F^{\lambda}_{L2}(Ri)] + \lambda_{\min} \tag{23}$$

for λ_T, where F^{λ}_{L2} is a decreasing function of the gradient Richardson number $Ri = N^2/M^2$.

2.4.4. *"Simple" Richardson number relations.* Early studies, e.g. Ekman (1905), of the effect of wind on thermocline depth recognized that the eddy diffusion coefficient must be smaller in stratified regions. Thus, using arguments based on dimensional analysis, simple formulae relating eddy diffusion coefficients to Richardson number were derived e.g. Munk and Anderson (1948). Such formulae have the advantage of computational simplicity compared to the higher level closure schemes of the preceding sections, while retaining a reduction of ν_T, λ_T in stratified regions. For example, a suitable shallow sea eddy viscosity form, e.g. Bowden (1978), can be extended to stratified flows by multiplying by $F(Ri)$, a function of Richardson number as suggested by Naimie *et al.* (1994). Such a formulation, e.g.

$$[\nu_T, \lambda_T] = 0.0025|\mathbf{U}|[F^{\nu}(Ri), F^{\lambda}(Ri)] + \lambda_{\min} \tag{24}$$

where $|\mathbf{U}|$ is the depth-integrated current, retains a similar dimensional form to (23) and simulates the variation of diffusion coefficients over the tidal cycle (though not depth).

An even simpler form (referred to hereafter as "PP") has been suggested by Pacanowski and Philander (1981)

$$\nu_T = \frac{\nu_{T_0}}{(1 + \alpha \max[0, Ri])^n} + \lambda_{\min} \tag{25}$$

$$\lambda_T = \frac{\nu_T}{1 + \alpha \max[0, Ri]} + \lambda_{\min}, \tag{26}$$

where the product of water depth and depth-averaged current has been substituted by a (dimensional) "neutral" diffusion coefficient.

In the present study this has been taken as $\nu_{T_0} = 10^{-2}$ m^2 s^{-1} (larger than that

in Pacanowski and Philander's original parameterization for the tropical ocean, since here we have, in the neutral case, strong turbulence generated by tidal currents over a rough bed in shallow water) and the empirical parameters are chosen as $n = 2$, $\alpha = 5$. Clearly one difficulty of this model lies in the calibration of these free, and, in the case of ν_{T_0}, dimensional parameters. Comparing (26) with (23) it is clear that PP represents less realistically turbulent processes since λ_T no longer depends on distance from the bottom/surface in a neutrally stratified boundary layer, nor on a time/velocity scale (as defined by e.g. a shear frequency or a friction velocity).

2.4.5. *Constant diffusion coefficients* (*CST*). Finally, many marine models are run with suitably chosen constant diffusion coefficients, e.g.

$$\lambda_T \equiv \nu_T \equiv 10^{-3}\ \mathrm{m^2\ s^{-1}}, \tag{27}$$

thus supposing that the extra expense of more complex turbulence closures is not justified by an accompanying increase in realism.

2.5. *Test conditions*

Owing to the considerable mesoscale variability described in Section 1.2 it seems impractical to model a long-time "average" salinity with any confidence. The approach adopted here is, therefore, to focus on how the freshwater plume reacts to idealized wind, tide and river discharge conditions, as defined by the boundary conditions given in Sections 2.6 and 2.7.

2.6. *Lateral boundary conditions*

The mode-splitting algorithm allows a natural decomposition between the depth-integrated velocity and its deviation, for which the respective boundary conditions are given in Sections 2.6.1 and 2.6.2.

2.6.1. *Barotropic mode at open sea boundaries*. Harmonic tidal predictions of surface elevation in the region use upwards of 20 harmonic constituents. However, thanks to the dominance of the M_2 tidal component, it is sufficient for this process study to consider only a single semi-diurnal component—little physics of interest is thus lost.

Open sea boundary conditions for the depth-integrated current $\mathbf{U} = (U, V)$ and the surface elevation η are designed by considering the propagation of Riemann variables, as suggested by Hedstrom (1979), Gerritsen (1982) and reviewed by Røed and Cooper (1987).

At the southwest open sea boundary $x = 0$, the incoming Riemann variable is imposed by (28), where the incoming tide is approximated as a frictionless Kelvin wave with angular frequency $\omega = 1.4056 * 10^{-4}\ \mathrm{s^{-1}}$, propagation speed, $c = \sqrt{gH}$, amplitude η_0, tuned to give realistic currents within the domain, and barotropic Rossby radius, $R_L = 122$ km; a radiation-type condition, derived by adding the depth-integrals of (5) and $-c * (3)$, is applied to the outgoing Riemann variable (29). The incoming and outgoing Riemann variables are then combined to give the normal transport $U_{x=0}$ at the boundary.

At the northeast open sea boundary $x = L_x$, the incoming Riemann variable is

supposed to have zero normal gradient (30). This is combined with a radiation-type condition for the outgoing Riemann variable (31).

$$U + c\eta|_{x=0} = 2c\eta_0 e^{-y/R_L} \sin \omega t \tag{28}$$

$$\left(\frac{\partial}{\partial t} - c\frac{\partial}{\partial x}\right)(U - c\eta)\Big|_{x=0} = + c\frac{\partial V}{\partial y} + \tau_x^s - \tau_x^b + fV - \hat{\mathcal{A}}_x^h + \hat{\mathcal{D}}_x^d \tag{29}$$

$$\frac{\partial}{\partial x}(U - c\eta)\Big|_{x=L_x} = 0 \tag{30}$$

$$\left(\frac{\partial}{\partial t} + c\frac{\partial}{\partial x}\right)(U + c\eta)\Big|_{x=L_x} = - c\frac{\partial V}{\partial y} + \tau_x^s - \tau_x^b + fV - \hat{\mathcal{A}}_x^h + \hat{\mathcal{D}}_x^d \tag{31}$$

where τ^s and τ^b are the surface and bottom stress, and $\hat{\mathcal{A}}^h$ and $\hat{\mathcal{D}}^d$ are the vertical integrals of horizontal advection of momentum and buoyancy-induced pressure gradient, respectively.

At the offshore boundary, since the distance from the coast is much less than a barotropic Rossby radius, the condition of zero cross-shore transport can be applied to good approximation,

$$V|_{y=L_y} = 0. \tag{32}$$

At the "estuary" boundary, 4 km from the river mouth, the volume flow is imposed via

$$V|_{y=0} = h(v_R + v_T \sin(\omega t - \phi)) \tag{33}$$

where $v_R = Q/(W_r h)$ is the depth-averaged current generated by the freshwater discharge. Setting river discharge, $Q = 1500\ \mathrm{m^3\ s^{-1}}$, for a river mouth width, $W_r = 10^3$m, and depth $h = 24$ m, gives river-induced depth-averaged current, $v_R \sim 0.06\ \mathrm{m\ s^{-1}}$.

In order to obtain maximum discharge at low water and current variation of about 1.2 m $\mathrm{s^{-1}}$ over the tidal cycle—as suggested by the measurements of van Alphen *et al.* (1988) and the tidal stream atlas produced by the Dutch Dienst Der Hydrografie (1992)—the tidally-induced depth-averaged current is imposed as $v_T = 0.6\ \mathrm{m\ s^{-1}}$ in the estuary, with phase $\phi = \pi + (\omega x/\bar{c})$ with respect to the left-hand boundary, where $\bar{c} = \sqrt{g\ 20\ \mathrm{m}}$ is a typical tidal wave propagation speed for the domain, and $x = 25$ km is the distance from the southwest open boundary.

2.6.2. *Vertical structure of currents at open sea boundaries*. The vertical structure at open sea boundaries ($x = 0, x = L_x, y = L_y$) is allowed to develop from the internal solution, by requiring zero normal derivative of the deviation from the vertically-averaged horizontal velocity as suggested by Deleersnijder *et al.* (1992), and given for the offshore boundary:

$$\frac{\partial}{\partial y}\left(v - \frac{V}{H}\right)\Big|_{y=L_y} = 0. \tag{34}$$

At the estuarine boundary however, such a condition would introduce a very strong dependence on current profiles within the domain, and, hence, the supply of potential energy to drive the plume would be very sensitive to v_T. Since the aim here is to compare parameterizations of turbulence for the river plume and not to model in detail the complex

mixing processes occurring in the estuary, the velocity deviation was instead imposed directly as a two layer estuarine-type circulation through

$$\left(v - \frac{V}{H}\right)\Big|_{y=0} = \begin{cases} +0.75\ \mathrm{m\,s^{-1}} & \text{for } z > 0.6H \\ -0.5\ \mathrm{m\,s^{-1}} & \text{for } z \le 0.6H, \end{cases} \tag{35}$$

with current directed out of the estuary at the surface and into the estuary at the bottom.

2.6.3. *Salinity at open sea boundaries.* Salinity is treated at open sea boundaries by upwinding when flux is out of the domain and by calculating the incoming flux either from an imposed vertical profile (36),(37),(39) or supposing zero horizontal derivative (38).

$$S|_{x=0} = S_0 \tag{36}$$

$$S|_{y=0} = \begin{cases} 10\ \mathrm{PSU} & \text{for } z > 0.6H - h \\ 22\ \mathrm{PSU} & \text{for } z \le 0.6H - h \end{cases} \tag{37}$$

$$\left.\frac{\partial S}{\partial x}\right|_{x=L_x} = 0 \tag{38}$$

$$S|_{y=L_y} = S_0. \tag{39}$$

2.7. *Surface and bottom boundary conditions*

Bottom stress, τ^b, is computed using a quadratic wall-function

$$\nu_T \left.\frac{\partial \mathbf{u}}{\partial z}\right|_{z=-h} = \tau^b = C_D \mathbf{u}_b |\mathbf{u}_b| \tag{40}$$

where $\mathbf{u}_b = \mathbf{u}|_{z=-h+\Delta z/2}$ is the near-bottom velocity, and C_D the drag coefficient

$$C_D = \left\{\frac{1}{\kappa} \log \frac{\Delta z/2}{z_0}\right\}^{-2} \tag{41}$$

is based on a roughness length, z_0 (see Table 1). Wind stress, τ^s, is imposed via

$$\nu_T \left.\frac{\partial \mathbf{u}}{\partial z}\right|_{z=+\eta} = \tau^s. \tag{42}$$

Zero flux surface and bottom boundary conditions are employed for salinity, and the conventional boundary layer conditions

$$k|_{z=-h,\eta} = |\boldsymbol{\tau}^{b,s}| \frac{B_1^{2/3}}{2} \tag{43}$$

$$kl|_{z=-h+\Delta z,\eta-\Delta z} = |\boldsymbol{\tau}^{b,s}| \frac{B_1^{2/3}}{2} \kappa \Delta z \tag{44}$$

are used for turbulent quantities.

2.8. *Initial conditions*

Initial conditions were obtained by spinning up the model for 20 tidal cycles from rest ($\mathbf{u} \equiv 0$, $S \equiv 0$), by which time $\mathbf{u}$ and S achieve an approximately periodic state.

3. RESULTS

A summary of the simulations for which results are presented can be found in Table 2.

3.1. *Tidally-averaged salinity distribution*

Results are first shown for the simulation with the "k" model (chosen as the "reference" model for reasons explained later), and for neap tide and no wind. The salinity and current fields are strongly coupled: freshwater from the river mouth is advected by currents, and currents are influenced by freshwater both through density-induced pressure gradients and through suppression of vertical diffusion of momentum by stratification. The effect of the salinity field on the residual current is seen in Fig. 3(a) and (b).

The tidally-averaged surface salinity field [Fig. 3(a)] shows the freshwater emerging from the mouth as a jet, and turning under the influence of the Coriolis force to attach to the coast, forming offshore of Noordwijk a coastal buoyancy current. This anticyclonic eddy and coastal current structure has been found for non-tidal river plumes, e.g. in the laboratory experiments of McClimans (1988), the primitive equation modelling of Chao and Boicourt (1986) and the layer model of Garvine (1987). The corresponding tidally-averaged elevation field [Fig. 3(b)] shows a raised surface elevation in the freshwater plume. To explain this the tidally-averaged depth-integrated pressure gradient Q can be decomposed into its surface elevation component, Q_η, and its buoyancy-induced component, Q_b, defined as

$$Q = -\int_{-h}^{+\eta} \nabla_h q \, \mathrm{d}z \tag{45}$$

$$= Q_\eta + Q_b \tag{46}$$

Table 2. Turbulence model, tidal amplitude and wind stress used in simulations (EQM = *"equilibrium"*; EVOL = *"evolution"*; PARA = *"parabolic"*)

Model	k-equation	l-equation	$\lambda_{\min}$ ($m^2 s^{-1}$)	Tide η_0 (m)	Wind τ($m^2 s^{-2}$)
k-kl	EVOL (8)	kl-EVOL (9)	10^{-4}	0.8	0
k (neap)	EVOL (8)	PARA (22)	10^{-4}	0.8	0
L2	EQM (23)	PARA (22)	10^{-4}	0.8	0
PP	(25,26)	(25,26)	10^{-4}	0.8	0
CST (10^{-3})	—	—	10^{-3}	0.8	0
k (spring)	EVOL (8)	PARA (22)	10^{-4}	1.1	0
k (SW wind I)	EVOL (8)	PARA (22)	10^{-4}	0.8	$(+2.2 * 10^{-5},0)$
k (SW wind II)	EVOL (8)	PARA (22)	10^{-4}	0.8	$(+10^{-4},0)$
k (NW wind)	EVOL (8)	PARA (22)	10^{-4}	0.8	$(0,-10^{-4})$

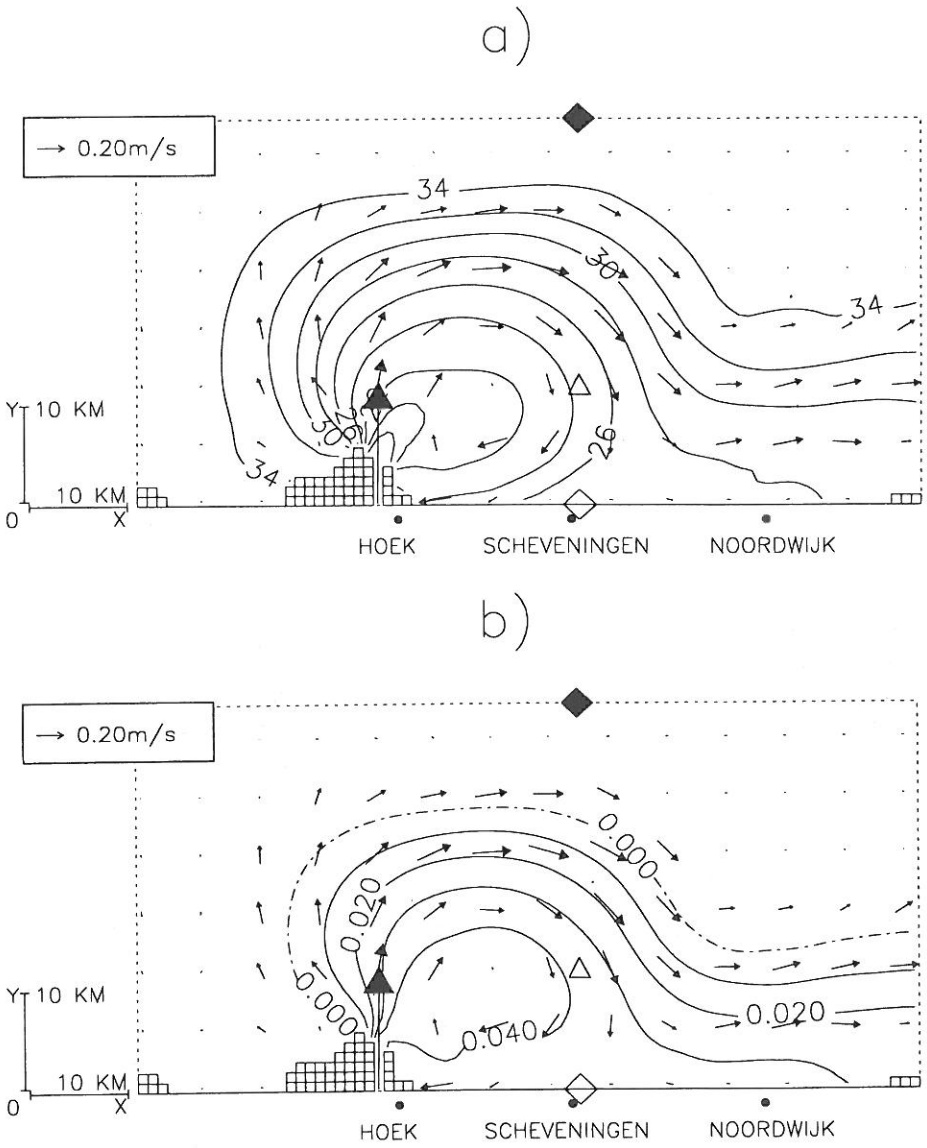

Fig. 3. Tidally-averaged surface current vectors (centered on cell) and contours of (a) surface salinity (in psu) and (b) surface elevation (in m). Neap tide, no wind, k model.

where

$$Q_\eta = -gH\nabla_h\eta \tag{47}$$

and

$$Q_b = -\int_{-h}^{+\eta} \nabla_h(q - g\eta)\mathrm{d}z. \tag{48}$$

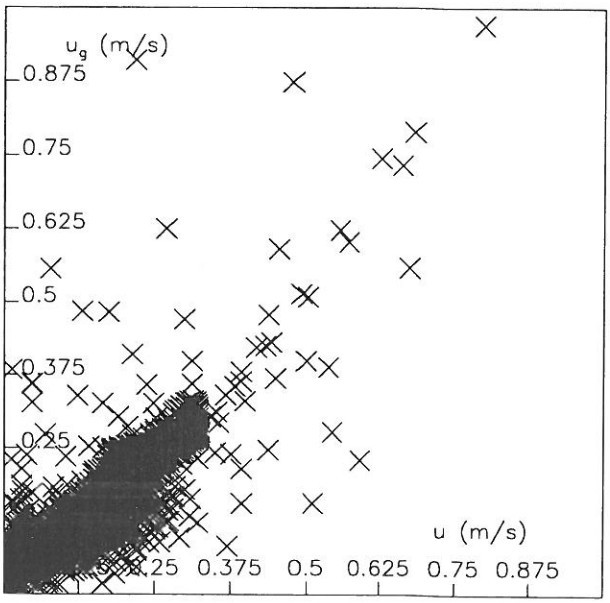

Fig. 4. Scattergram of surface current against geostrophic component of surface current.

Calculation of the norms of these two terms over the domain via

$$\|Q_\eta\| = \frac{\Sigma Q_\eta}{\Sigma 1} \tag{49}$$

where the summation is taken over all the points in the domain except those adjacent to boundaries, yields $\|Q_\eta\| = 2.8 * 10^{-4}\ \mathrm{m^2\,s^{-2}}$ and $\|Q_\eta + Q_b\| = 7.7 * 10^{-5}\ \mathrm{m^2\,s^{-2}}$. The two pressure gradient terms, Q_b and Q_η are by far the largest terms in the depth-integrated momentum equation and they cancel approximately (with the difference made up by all the other much smaller terms: bottom stress, advection of momentum, time variation and Coriolis). This rather striking property is similar, though not identical, to the concept of isostasy, e.g. Garvine (1987).

The tidally-averaged surface current field is seen to lie approximately parallel to the elevation contours. A scattergram (Fig. 4) of the magnitude of the geostrophic component of surface current, u_g—defined

$$f\mathbf{e}_z \otimes \mathbf{u}_g = -\nabla_h q \tag{50}$$

by retaining only the Coriolis and pressure gradient terms of the full momentum equation (5)—against the actual surface current suggests an approximately geostrophic balance. It is remarkable that a nearly geostrophic flow arises from averaging over the strong semi-diurnal variability. The contribution from the averaging of the non-linear terms on the left-hand side of (5) is small except near the river mouth, where the characteristic length scale is smaller since determined by the width of the river mouth (Garvine, 1987). The surface residual current is similarly little affected by vertical diffusion of momentum, since the strong stratification suppresses such mixing, and the surface layer slips almost frictionless over the lower layer fluid.

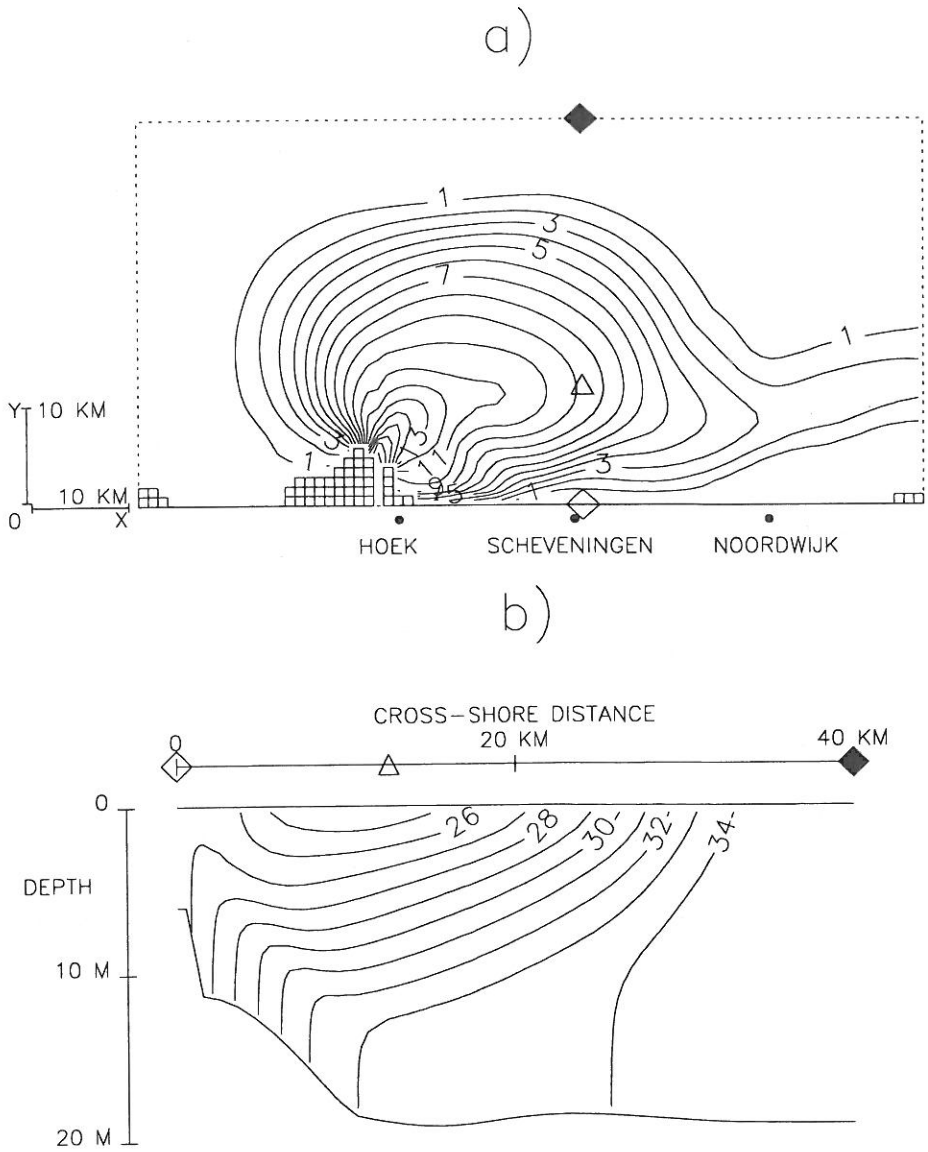

Fig. 5. Contours of tidally-averaged (a) bottom-surface salinity (in psu) and (b) salinity (in psu) for the Scheveningen cross-shore transect. Neap tide, no wind, k model.

The stratification, defined as the bottom-surface salinity difference, is plotted in Fig. 5(a). A cross-shore transect taken through the plume near Scheveningen [Fig. 5(b)] shows that the salinity field has a clear two layer structure: the bottom layer is well-mixed with near-vertical bottoming isopycnals, while the surface layer is strongly and continuously stratified forming a "lens" of freshwater extending to about 30 km offshore (not, however, bounded by a sharp front since tidal-averaging and low grid resolution tend to smear such features). Such a bottom-mixed surface-stratified structure is sometimes found on CTD

measurements in this region (e.g. Fig. 8 of de Ruijter *et al.* 1992): turbulence generated by shearing of the tidal current over the bottom mixes salinity in the bottom layer. The surface layer is continuously stratified for the no wind case (as simulated here) or mixed with a sharp pycnocline separation from the bottom mixed layer in the presence of wind.

The (first) baroclinic Rossby radius, R_I is estimated

$$R_I = \frac{1}{f}\sqrt{\frac{g\beta_S \Delta S h_u (h - h_u)}{h}} \sim 4 \text{ km} \tag{51}$$

by approximating as a two layer system (e.g. Gill 1982) with upper layer thickness, $h_u \sim 15$ m and salinity difference between the two layers, $\Delta S \sim 6$ psu, estimated *a posteriori* from model results and taking $h \sim 20$ m.

The anticyclonic eddy radius and the width of the ensuing coastal current are seen to be about two to four times larger than R_I, the characteristic length scale for a rotating frictionless plume. While Stern *et al.* (1982) suggest that the inviscid limit gives a coastal jet of width $0.4\,R_I$, Chao (1988) claims that diffusive plumes are significantly wider, as found here.

The time series of along-shore and cross-shore currents at a "mooring" in the plume 13 km offshore of Scheveningen (marked as △ on Figs 1 and 2) is shown in Fig. 6. The along-shore currents show strong vertical shear even in the surface layer (since momentum is only weakly mixed vertically by turbulent viscosity) and the asymmetry between flood and ebb tides indicates a strongly-sheared residual current (generated by the horizontal density gradient). The cross-shore currents are approximately 90° out of phase with the along-shore currents and tend to show oppositely directed surface and bottom currents (as well as a residual component), as found in the measurements described by Visser *et al.* (1994).

3.2. *Sensitivity of tidally-averaged salinity to parameterization of vertical mixing*

It is difficult to test the results of the previous section by comparison with measured salinity fields, since any "good agreement" found may result from a fortuitous choice of data and any discrepancy between model results and data may arise from either deficiencies in the model or insufficient knowledge of initial and/or boundary conditions (especially at the river mouth), neither of which are provided simultaneously during measurement campaigns. Therefore, considering the complexity of the task of modelling stratified flows the aim here has been more modest: to assess the sensitivity of results to model parameters, in particular the turbulence model, and to wind and tide forcing. Such a study provides an essential precursor to future studies where a closer comparison with data is hoped for.

Figures 7 and 8 shows the results for the same simulation performed using the "k–kl" and "level 2" turbulence models. Clearly as far as the tidally-averaged salinity field is concerned there are only small differences between the "k–kl" and "k" models. For the "k–kl" model this can be explained by considering that in the bottom shear layer the asymptotic form as $z \to -h$ in (9) gives a linear dependence of l on d_b as in (22), and in the strongly stratified surface layer $\nu_T = \lambda_T = \lambda_{\min}$.

Figures 9 and 10 show for the "k" and the level 2 models respectively, the time and depth variation of ν_T over a tidal cycle at the "mooring". For both models ν_T is very small (in fact often equal to the threshold $\nu_{\min}$) for the upper 10 m throughout the tidal cycle.

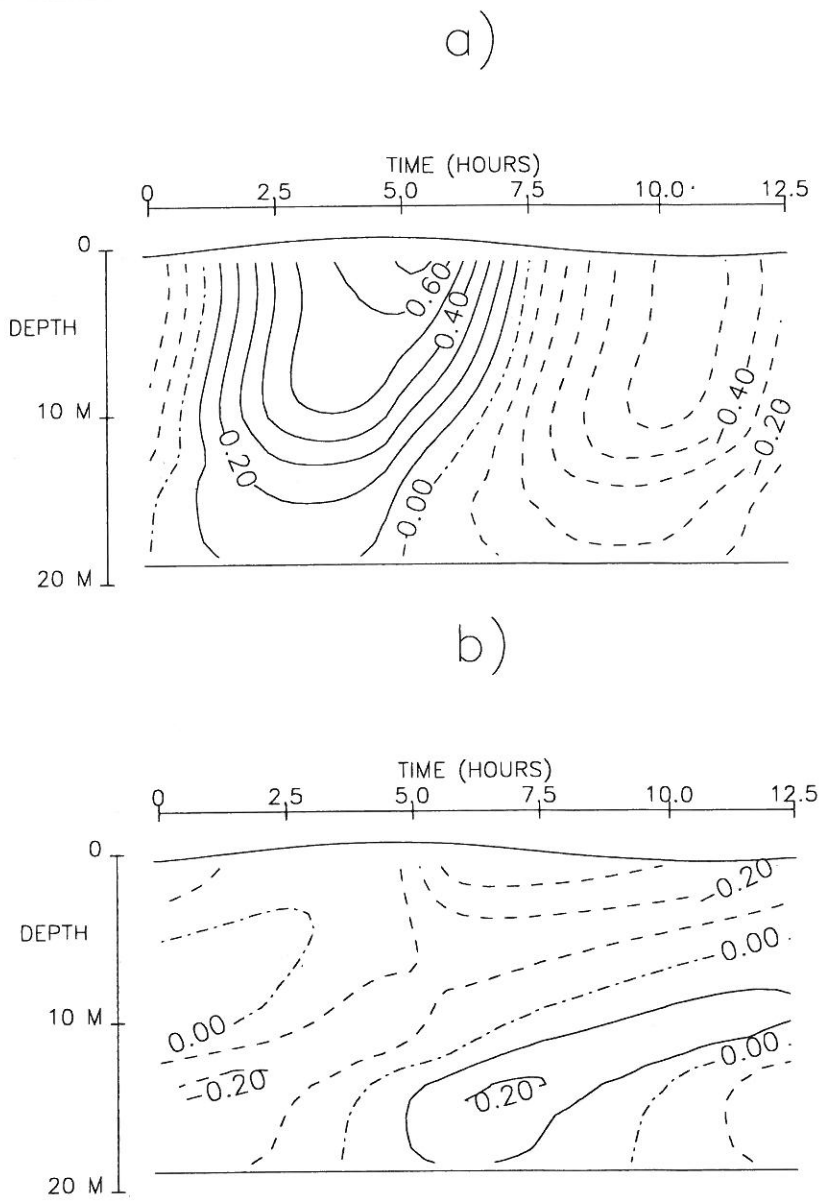

Fig. 6. Contours of (a) along-shore current, u, (in m s^{-1}, >0 to NE) and (b) cross-shore current, v, (in m s^{-1}, >0 offshore) for the "mooring" △ 13 km offshore of Scheveningen. Neap tide, no wind, k model.

Tidal-mixing generates peaks of ν_T in the bottom 5 m near the moments of maximum alongshore current. For the level 2 model ν_T is dominated by $2\Delta t$ oscillations—this erratic or "noisy" behaviour of the level 2 diffusion coefficients has been noted by other investigators (e.g. Frey, 1991). Interestingly the salinity field is not disastrously contaminated, perhaps because in the bottom shear layer isolated peaks of λ_T change little, since

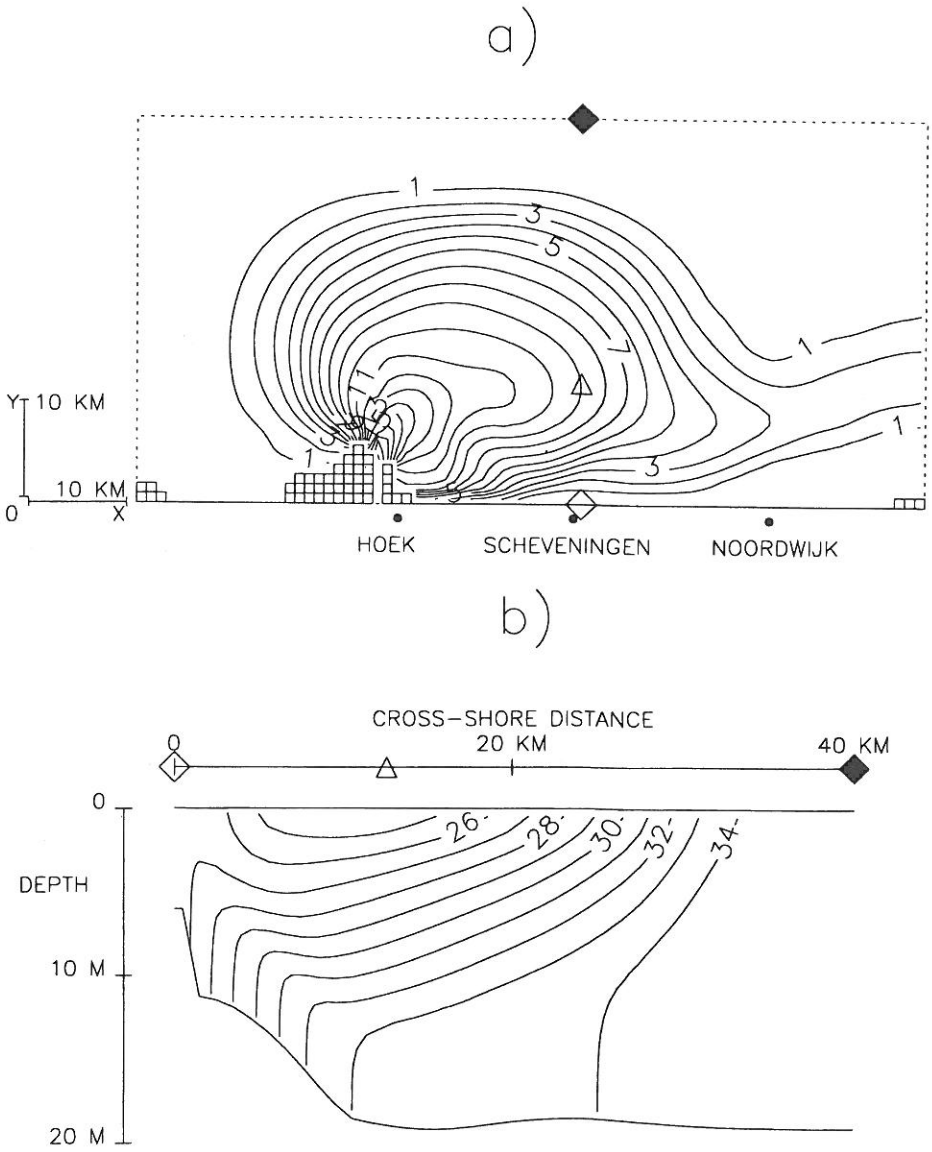

Fig. 7. Contours of tidally-averaged (a) bottom-surface salinity (in psu) and (b) salinity (in psu) for the Scheveningen cross-shore transect. Neap tide, no wind, *k–kl* model.

the salinity is already well-mixed here. Similarly, while velocity profiles may appear similar for the two models, the "noisy" nature of the level 2 model becomes apparent if derived quantities such as M^2 are inspected. Preliminary simulations performed with $\Delta t_{3D} = 60$ s and only 10 σ-layers gave considerably less noise, supporting the belief that such problems become more serious for increasing $\Delta t/\Delta z^2$ (Frey, 1991; Luyten *et al.*, 1995). This, and the fact that this problem appears as $2\Delta t$ oscillation and does not occur for, say, the PP

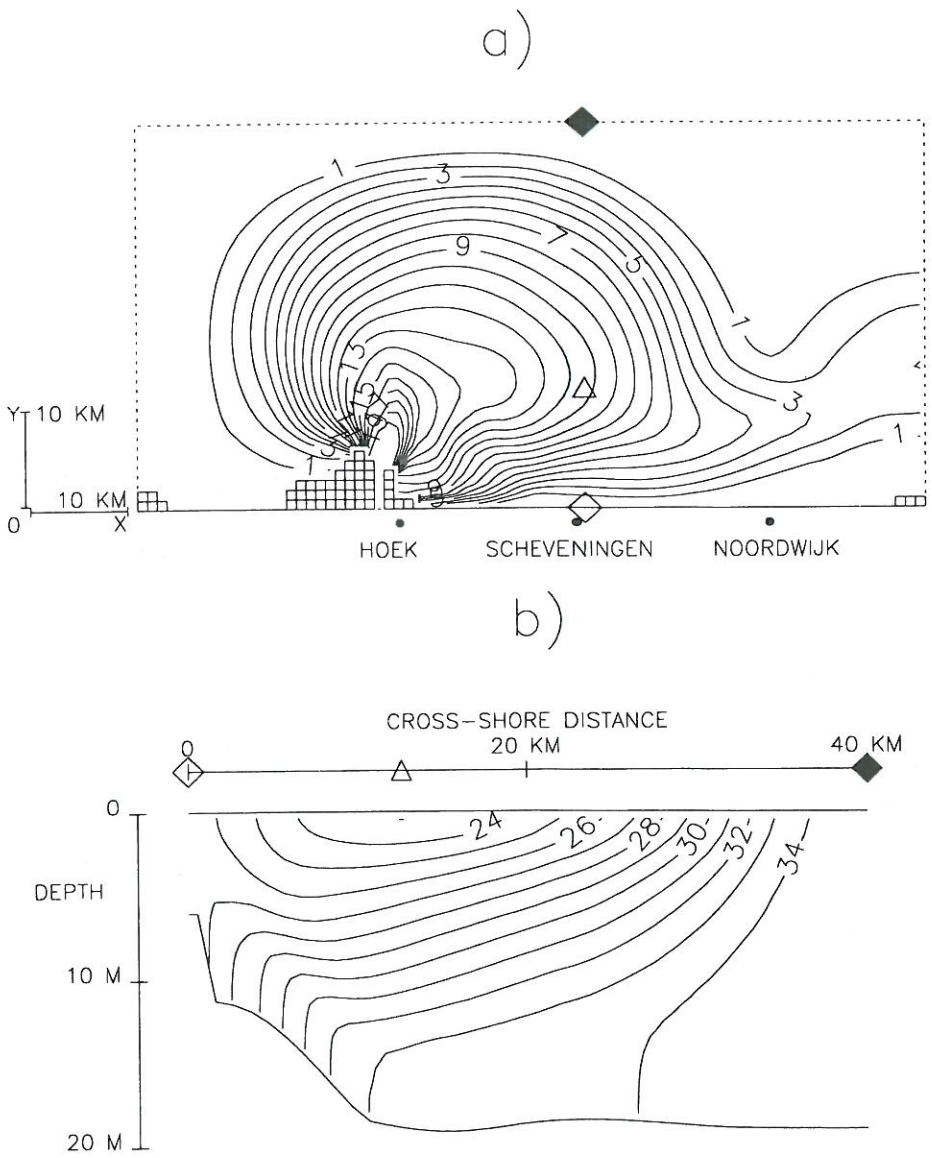

Fig. 8. Contours of tidally-averaged (a) bottom-surface salinity (in psu) and (b) salinity (in psu) for the Scheveningen cross-shore transect. Neap tide, no wind, level 2 model.

model, suggest that the cause may be a numerical instability associated with the explicit time discretization of ν_T in (5) and M in (23).

The tidally-averaged salinity field found with the PP model (Fig. 11) is qualitatively similar (quasi-geostrophic gyre, coastal current, bottom-mixed layer), though with differences of the order of 1 – 2 psu and cross-shore displacement of the plume boundary by a few kilometres with respect to the simulations with higher level turbulence closure. Comparing (26) with (23), where l and M may vary in space and time rather than being

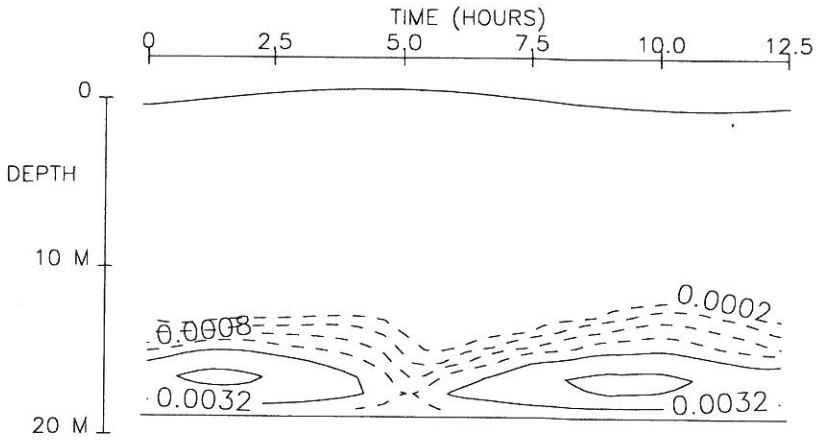

Fig. 9. Contours of ν_T (in $m^2\ s^{-1}$, drawn for $\nu_T = 2^n * 10^{-4}\ m^2\ s^{-1}$, $n = 1, 2, 3, \ldots$ with $\nu_T \leqslant 1.6 * 10^{-3}\ m^2\ s^{-1}$ as dashed contour) for the "mooring" $\triangle$ 13 km offshore of Scheveningen for simulation with Neap tide, no wind, k model. $\nu_{min} = 10^{-4}\ m^2\ s^{-1}$.

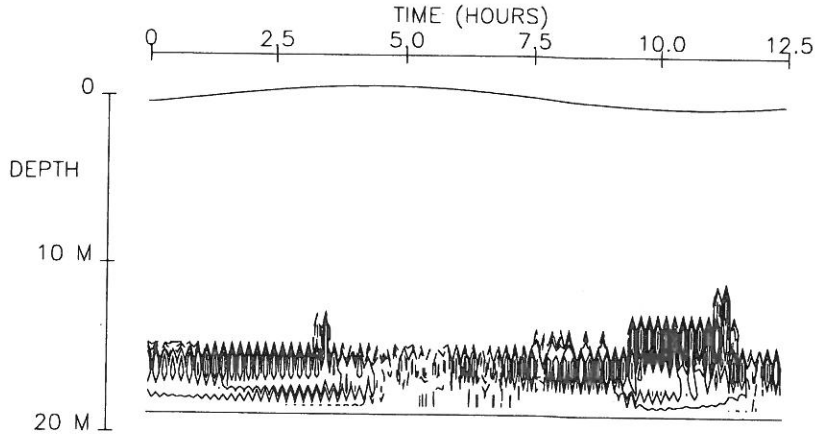

Fig. 10. Contours of ν_T (in $m^2\ s^{-1}$, drawn for $\nu_T = 2^n * 10^{-4}\ m^2\ s^{-1}$, $n = 1, 2, 3, \ldots$ with $\nu_T \leqslant 1.6 * 10^{3}\ m^2\ s^{-1}$ as dashed contour) for the "mooring" $\triangle$ 13 km offshore of Scheveningen for simulation with Neap tide, no wind, level 2 model. $\nu_{min} = 10^{-4}\ m^2\ s^{-1}$.

fixed via a neutral value ν_{T_0} it is perhaps surprising that these models do not give more greatly different salinity fields. In part this can be explained by the fact that in the stratified upper layer both models revert to the background mixing coefficients, while in the lower layer both models give a sufficiently large λ_T to achieve almost complete mixing of the bottom layer at the times of large tidal current.

Further simulations (not shown) with the formulation (24) suggest similar results provided the same functional form for F is taken. Simulations with the more diffusive Munk and Anderson (1948) form for F (which gives a reduction of λ_T by only a factor of 9 for $Ri = 1$) give a nearly well-mixed salinity field for the Scheveningen transect, which is

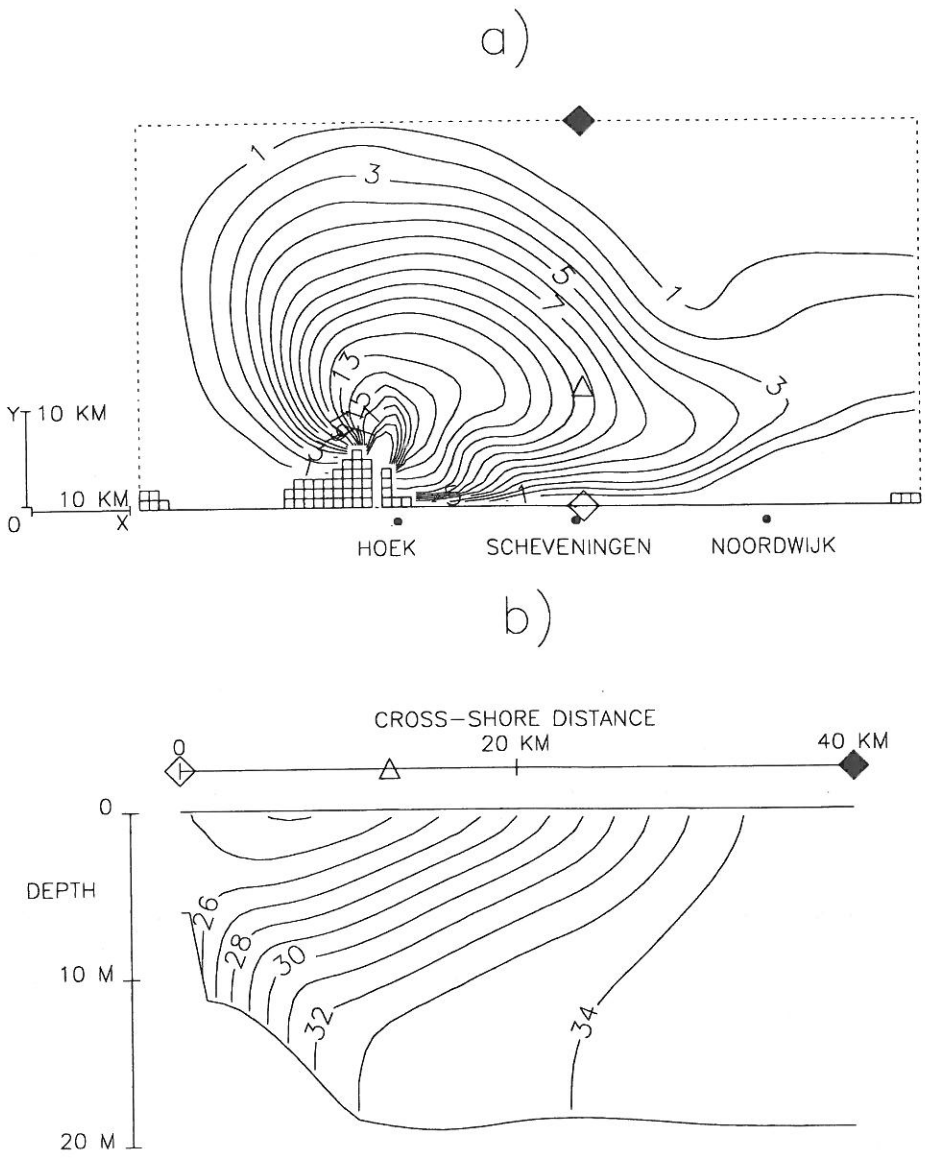

Fig. 11. Contours of tidally-averaged (a) bottom-surface salinity (in psu) and (b) salinity (in psu) for the Scheveningen cross-shore transect. Neap tide, no wind, PP model.

clearly unrealistic for a no wind case—compared to e.g. the measurements of van Alphen *et al.* (1988). Thus, while the PP model performed adequately in the present study, where stratification is strong, there is a danger that this model is sensitive to the calibration of the various parameters, especially n.

Simulations with constant diffusion coefficients show, not surprisingly, a drastically different salinity distribution compared to the k model. Taking $\nu_T = \lambda_T = 10^{-3}$ m^2 s^{-1}, stratification, shown in Fig. 12(a), is rapidly mixed away as the plume spreads along the

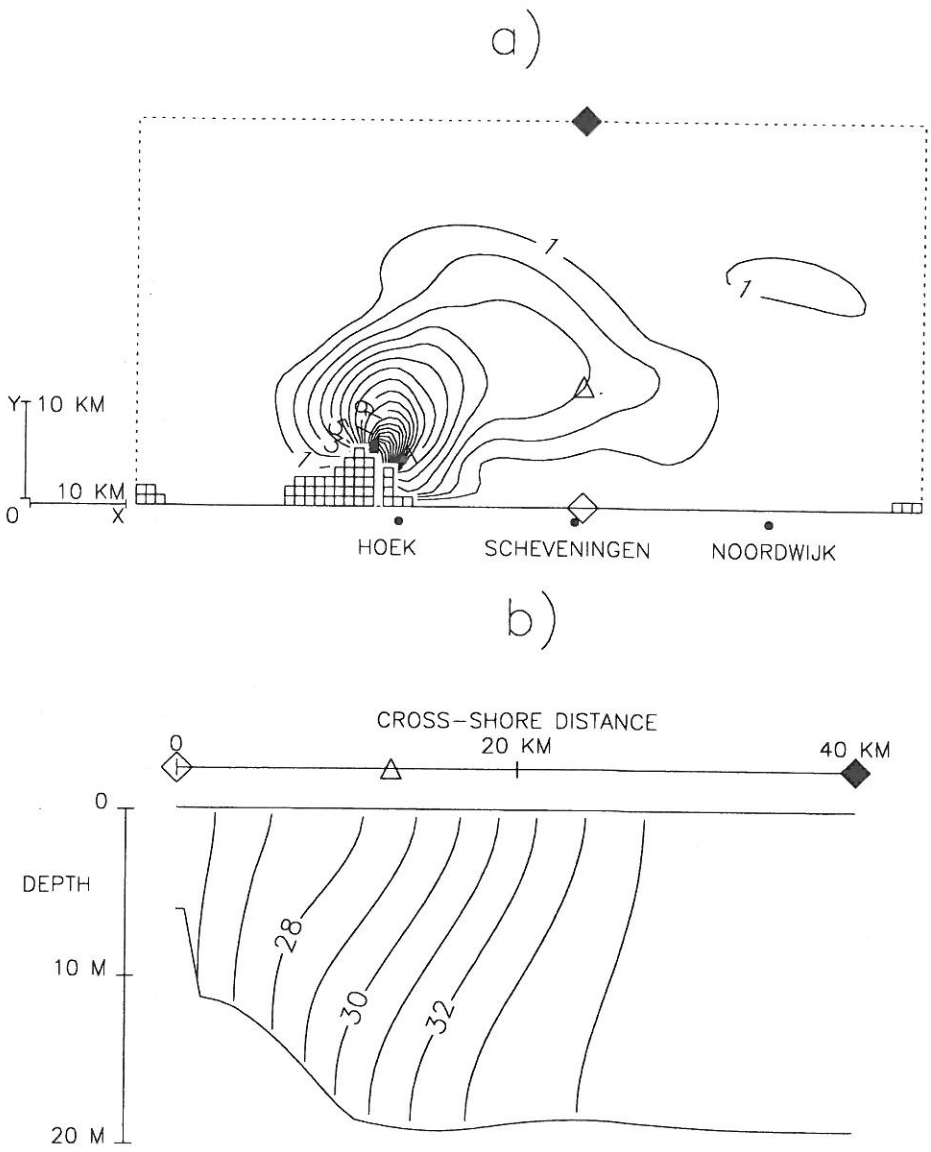

Fig. 12. Contours of tidally-averaged (a) bottom-surface salinity (in psu) and (b) salinity (in psu) for the Scheveningen cross-shore transect. Neap tide, no wind, $\nu_T = \lambda_T = 10^{-3}\,\mathrm{m^2\,s^{-1}}$.

coast, with an unrealistically well-mixed distribution (in the absence of wind) found offshore of Noordwijk. Cross-shore structure of the plume, Fig. 12(b), shows a weak stratification extending fairly continuously from surface to bottom in contrast to the two layer structure found previously. Clearly it is not possible to represent a bottom-mixed surface-stratified flow with constant diffusion coefficients. More seriously, the salinity field is extremely sensitive to calibration of these coefficients as found in results (not shown) of a simulation with $\nu_T = \lambda_T = 10^{-2}\,\mathrm{m^2\,s^{-1}}$—where the salinity field was vertically

well-mixed except for a small (5 km) region around the river mouth. The simple model of Appendix A indicates a strong dependence of stratification on λ_T.

3.3. *Sensitivity of tidally-averaged salinity to other modelling factors*

In the preceding section the constant diffusion coefficient was found unsuitable because of strong sensitivity of the solution to the choice of this coefficient, which in reality would be expected to vary in horizontal (stratified to well-mixed) and vertical (boundary layer) space and in time as tidal mixing generates turbulence by shear and advection of salinity influences stratification. However, the physically more realistic "k" model also requires calibration of the "background" mixing coefficient $\lambda_{\min}$. A further test (not shown here) with $\lambda_{\min} = 5 * 10^{-5}$ m^2 s^{-1} shows that stratification in the far-field does indeed depend to some extent (2 or 3 psu) on the choice of $\lambda_{\min}$. In effect $\lambda_{\min}$ is controlling $\partial s/\partial z$ in the stratified upper layer. Thus the turbulence closure calibration problem has been reduced, but not entirely eliminated. A test with low wind (2 m s^{-1}) and with only molecular background diffusion gave unrealistically low salinities of 18 psu up to the northeast boundary, suggesting that the background mixing coefficient is not only necessary for no wind simulations.

The algebraic length scale formulation (22) does not allow for a continuous reduction in the size of turbulent eddies by stratification—only an abrupt limitation via (18). To investigate the effect of this simplification, a simulation was performed with the "stratification damped" length scale of Panofsky (1963). However, there was no discernible difference in the salinity field, since such a modification only has effect in regions of strong stratification, where diffusion coefficients are already strongly reduced by suppression of k and by small values of the stability functions S_u, S_b.

A further simulation with a finer grid (Δx, Δy, Δt halved) gave similar results, though some grid dependence, especially in the poorly resolved river mouth region, gave salinities ~ 2 psu fresher in the upper layer.

Surprisingly a simulation with a much more diffusive first-order advection scheme gave qualitatively similar results—again differences of 1 or 2 psu were observed in the upper layer, but the flow field was not greatly different.

Finally a simulation with an "idealized" bathymetry (sloping rapidly to 22 m with isobaths perfectly parallel to the coast) gave a qualitatively similar flow field.

3.4. *Sensitivity of tidally-averaged salinity to tidal-forcing*

As mentioned in Section 1.2.1, while M_2 is the dominant tidal component, a spring–neap cycle is also present as seen in the current measurements of Simpson *et al.* (1993) [Fig. 4(a)]. A time series was also obtained [Simpson *et al.* 1993, Fig. 4(c)] showing switching between well-mixed at springs and stratified at neaps, though whether this could be attributed to the semi-monthly tidal mixing signal or to the strong wind found coincidentally at springs was uncertain, and was partly the inspiration for the simulation reported in this section. The measurements of van der Giessen *et al.* (1990) also show considerable spring–neap variability of the bottom and surface tidal current ellipses. Since the simulations reported in Sections 3.1 and 3.2 were designed to identify a typical tidally-averaged salinity field and test its sensitivity to the parameterization of vertical mixing only a single semi-diurnal component was used, thus enabling periodic solutions to be obtained at minimal computation. To assess the response of the residual salinity field to variation in

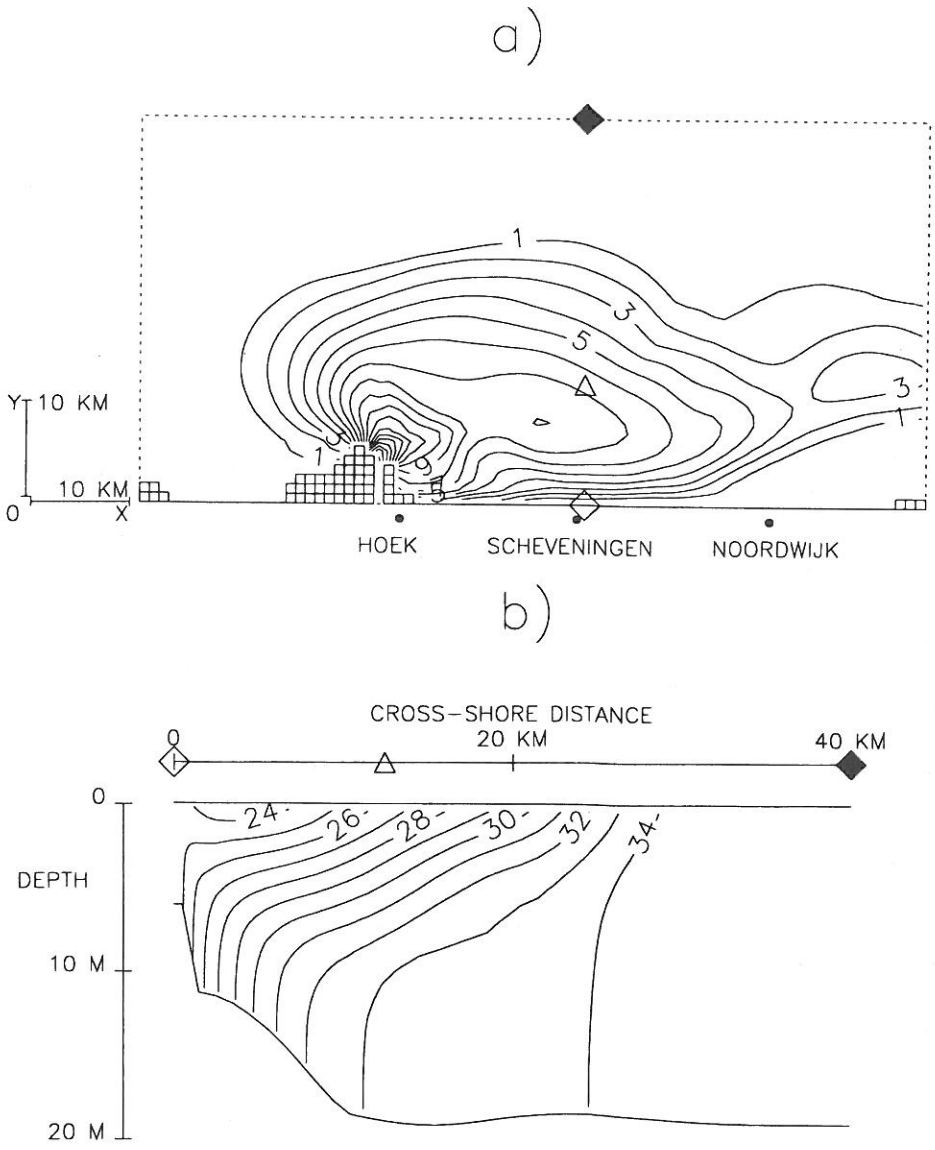

Fig. 13. Contours of tidally-averaged (a) bottom-surface salinity (in psu) and (b) salinity (in psu) for the Scheveningen cross-shore transect. Spring tide, no wind, k model.

the tidal forcing over the springs–neaps cycle a further simulation has been performed for a spring tidal amplitude $\eta_0 = 1.1$ m instead of $\eta_0 = 0.8$ m used previously. Since $U \sim c\eta$, currents will change approximately linearly with η_0.

Figure 13 shows the stratification and cross-shore structure of salinity for this spring tide simulation. Comparing with the neap tide "reference" simulation of Section 3.1, Fig. 5, a qualitatively similar salinity field is found, with less overall stratification, less cross-shore penetration of the outflow jet, and a thicker bottom-mixed layer. Various studies suggest that the thickness of a bottom-mixed layer, h_{BBL}, is given by

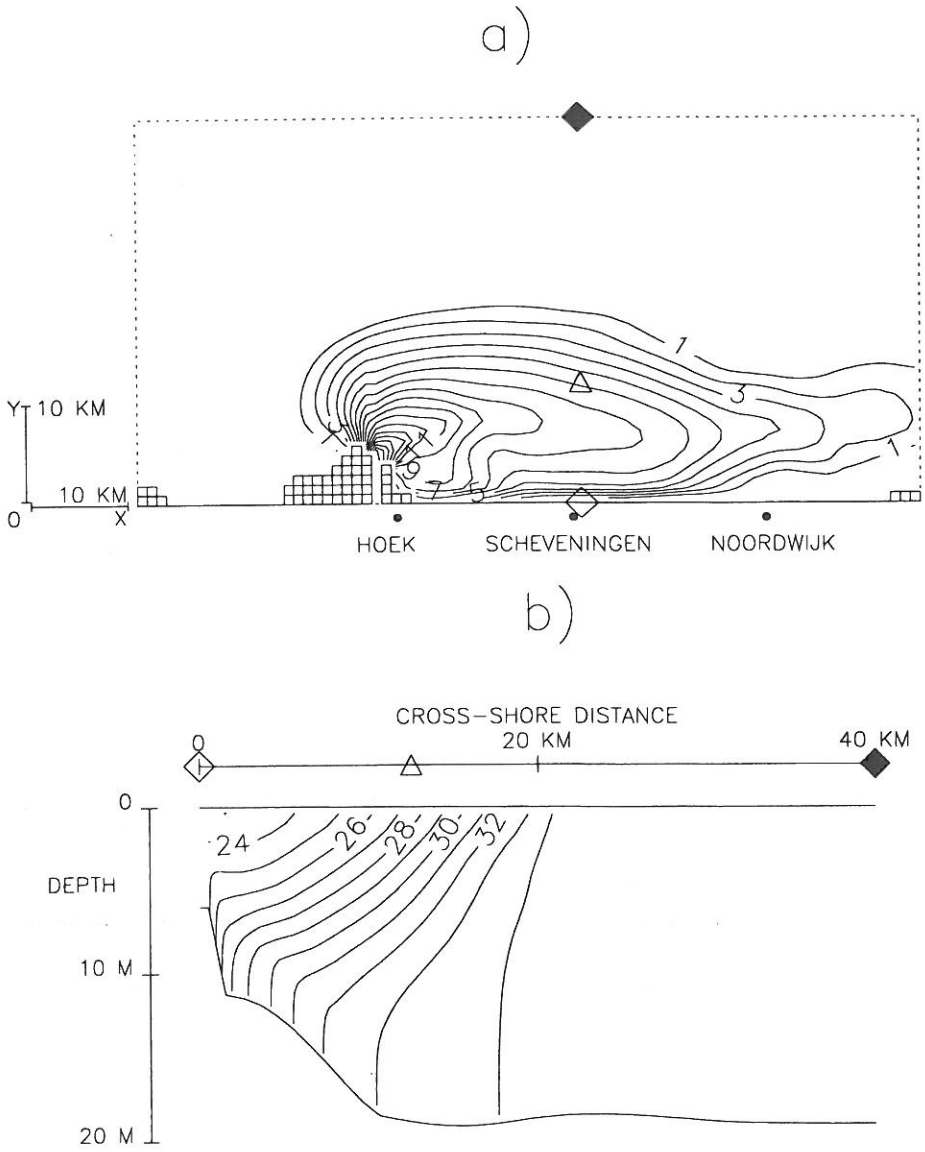

Fig. 14. Contours of tidally-averaged (a) bottom-surface salinity (in psu) and (b) salinity (in psu) for the Scheveningen cross-shore transect. Neap tide, along-shore (southwesterly) wind $\tau = (+2.2 * 10^{-5}\ \mathrm{m^2\,s^{-2}}, 0)$, k model.

$$h_{BBL} = u_* \gamma(f, \omega, N) \tag{52}$$

where $u_* = \sqrt{\tau^b}$ is the friction velocity, and γ is a suitable function of Coriolis, tidal and buoyancy frequencies, e.g. Weatherley and Martin (1978), Kitaigorodskii (1992). It may then be expected that the depth of a tidally-mixed bottom boundary layer is roughly proportional to the depth-averaged tidal current U/H and, thus, the tidal amplitude, η_0.

The small closed contour in Fig. 13(a) arises from tidal pulsing of the discharge.

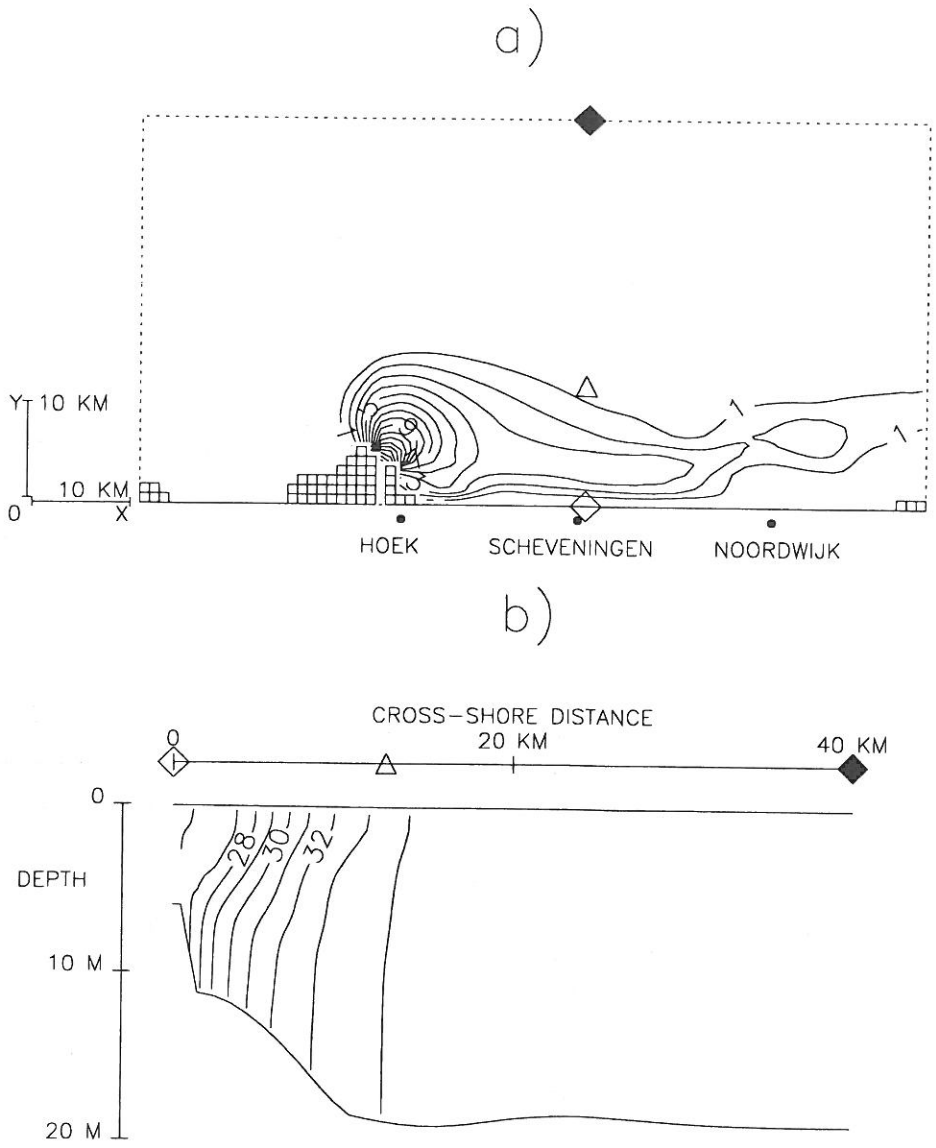

Fig. 15. Contours of tidally-averaged (a) bottom-surface salinity (in psu) and (b) salinity (in psu) for the Scheveningen cross-shore transect. Neap tide, along-shore (southwesterly) wind $\tau = (+10^{-4}\ \mathrm{m^2\ s^{-2}}, 0)$, k model.

3.5. *Sensitivity of tidally-averaged salinity to wind-forcing*

The simulations of the previous section were made with zero wind stress, and may thus be representative of periods of "low wind". Three further simulations were performed to determine how sensitive the plume is to wind, i.e. just how "low" should wind be for the preceding simulations to be valid and what is the influence of wind direction?

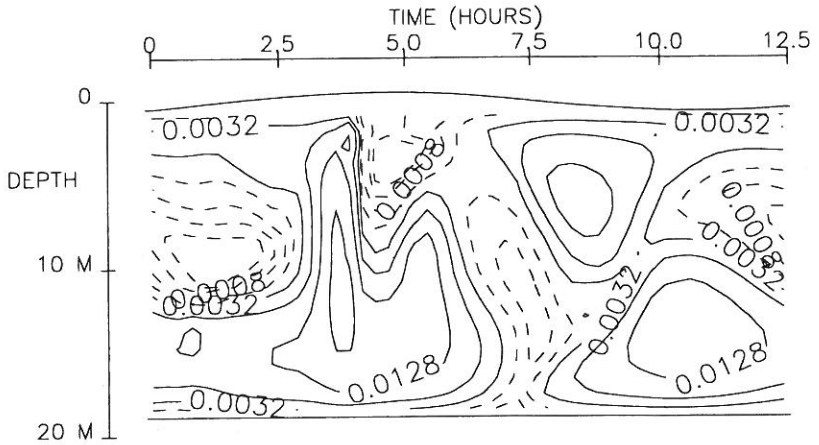

Fig. 16. Contours of ν_T (in $m^2\ s^{-1}$, drawn for $\nu_T = 2^n * 10^{-4}\ m^2\ s^{-1}$, $n = 1, 2, 3, \ldots$ with $\nu_T \leq 1.6 * 10^{-3}\ m^2\ s^{-1}$ as dashed contour) for the "mooring" Δ 13 km offshore of Scheveningen. $\nu_{min} = 10^{-4}\ m^2\ s^{-1}$. Neap tide, along-shore (southwesterly) wind $\tau = (+10^{-4}\ m^2\ s^{-2}, 0)$, k model.

Figure 14 shows the stratification and cross-shore salinity structure for a simulation of neap tide with a "k" model and an along-shore (southwesterly) wind stress of $2.2 * 10^{-5}\ m^2\ s^{-2}$ [corresponding to a wind speed at a height of 10 m of about $4.5\ m\ s^{-1}$ supposing a Smith and Banke (1975) wind drag formulation]. Compared with the no wind simulation of Fig. 5 cross-shore penetration is reduced and overall stratification is reduced.

For a stronger along-shore wind stress of $10^{-4}\ m^2\ s^{-2}$ (corresponding to a wind speed of about $8.5\ m\ s^{-1}$—common for this region) the stratification (Fig. 15) is significantly reduced by wind-mixing and the plume is confined to a coastal band 10 km wide. Tidally-averaged surface velocities within the plume are high since both wind and density effects generate along-shore flow. The time series of ν_T at the "mooring" (Fig. 16) shows that ν_T is now fairly large throughout the water column—the quarter-diurnal bottom-mixing signal penetrates more than 10 m and wind-mixing is apparent in the surface layer. The time variation of ν_T is strongly influenced by de- and restratification caused by semi-diurnal tidal straining of the salinity field—a similar effect was found in Liverpool Bay by Sharples and Simpson (1995).

The plume is also highly sensitive to wind direction. Figure 17 shows the stratification and cross-shore salinity for an onshore (northwesterly) wind stress of $10^{-4}\ m^2\ s^{-2}$. The onshore wind tends to reduce stratification both by increasing mixing and by inducing onshore surface current. The wind-mixed surface layer and tidally-mixed bottom layer are separated by an intermediate layer of strong stratification. In the case of an offshore wind (results not shown) the plume is blown offshore.

4. CONCLUSIONS

The tidally-averaged salinity field in the region of the Rhine–Meuse plume has been studied using a three-dimensional numerical model. A "control" simulation (using a

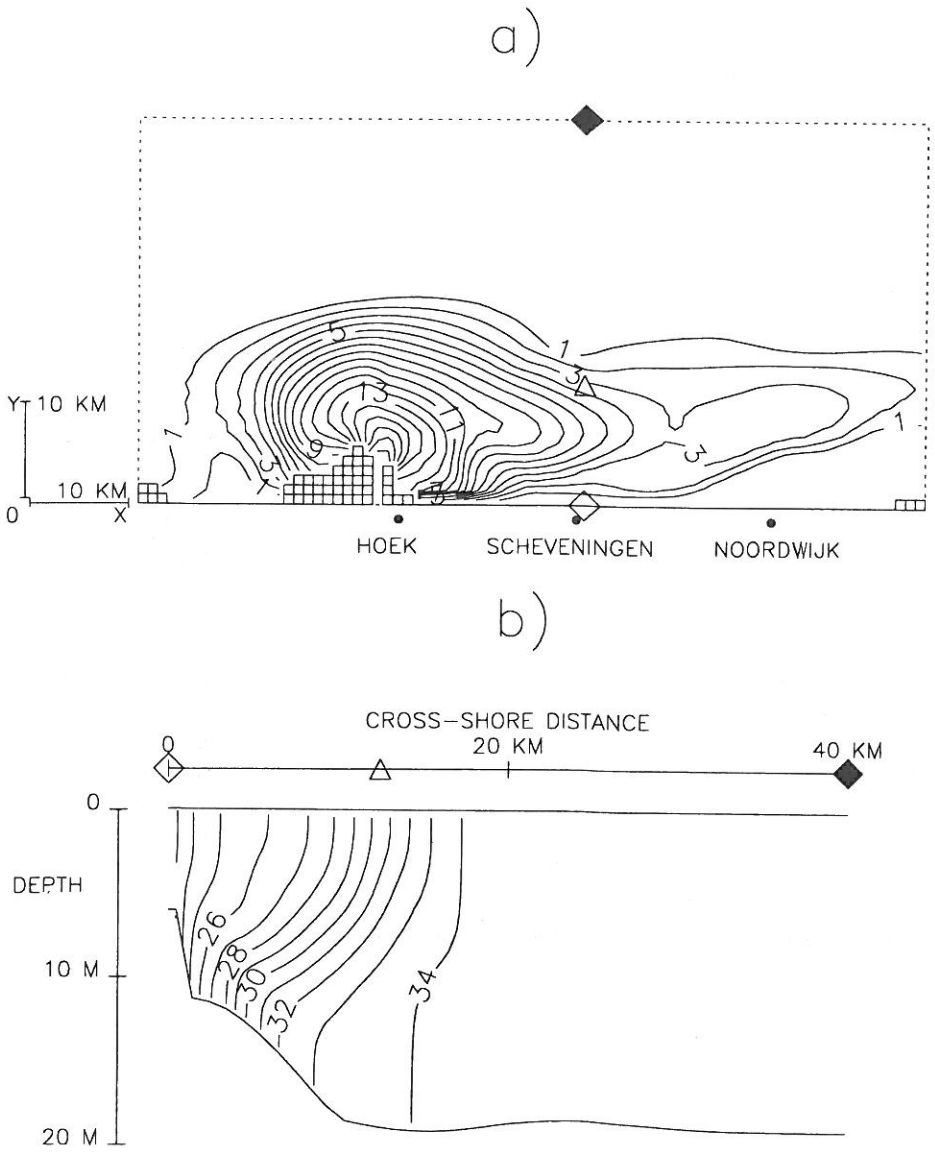

Fig. 17. Contours of tidally-averaged (a) bottom-surface salinity (in psu) and (b) salinity (in psu) for the Scheveningen cross-shore transect. Neap tide, on-shore (northwesterly) wind $\tau = (0, -10^{-4}\ \mathrm{m^2\ s^{-2}})$, k model.

turbulence closure with evolution equation for turbulent kinetic energy and stratification-dependent stability functions) shows the plume as a fresh-water jet turning right under the influence of Coriolis force to form a coastal buoyancy current. Surface residual currents are essentially geostrophic and density-driven with magnitude $\sim 0.2\ \mathrm{m\ s^{-1}}$. Within the plume the surface layer is continuously and strongly stratified and overlies a bottom mixed

Heaps N. S., editor (1987) *Three-dimensional coastal ocean models*. American Geophysical Union, Washington D.C., p. 208.

Hedstrom G. W. (1979) Nonreflecting boundary conditions for non-linear hyperbolic systems. *Journal of Computational Physics*, **30**, 222–237.

Hopfinger E. J. (1987) Turbulence in stratified fluids: a review. *Journal of Geophysical Research*, **92**(C5), 5287–5303.

James I. D. (1986) A front-resolving sigma coordinate sea model with a simple hybrid advection scheme. *Applied Mathematical Modelling*, **10**, 87–92.

Kitaigorodskii S. A. (1992) The location of thermal shelf fronts and the variability of heights of tidal benthic boundary layers. *Tellus*, **44A**(5), 425–433.

Laane R. W. P. M., J. Van Der Meer, A. De Vries and A. Van Der Giessen (1989) *Monitoring the reduction of the attempts to reduce nutrient load and inputs of certain compounds in the North Sea by* 50%. Report GWAO 89.008, Rijkswaterstaat Dienst Getijdwateren, P.O. Box 20904, 2500 EX, Den Haag, Netherlands.

Luyten P. J., E. Deleersnijder, J. Ozer and K. G. Ruddick (1995) Presentation of a family of turbulence closure models for stratified shallow water flows and preliminary application to the Rhine outflow region. *Continental Shelf Research*.

Martin P. J. (1985) Simulation of the mixed layer at OWS November and Papa with several models. *Journal of Geophysical Research*, **90**(C1), 903–916.

McClimans T. A. (1988) Estuarine fronts and river plumes. In: *Physical processes in estuaries*, J. Dronkers and W. van Leussen, editors, Springer-Verlag, pp. 55–69.

Mellor G. L. (1985) Ensemble averaged turbulence closure. *Advances in Geophysics*, **28B**, 345–358.

Mellor G. L. and T. Yamada (1974) A hierarchy of turbulent closure models for planetary boundary layers. *Journal of Atmospheric Sciences*, **31**, 1791–1806.

Mellor G. L. and T. Yamada (1982) Development of a turbulent closure model for geophysical fluid problems. *Reviews in Geophysics and Space Physics*, **20**, 851–875.

Munk W. H. and E. R. Anderson (1948) Notes on a theory of the thermocline. *Journal of Marine Research*, **VII**(3), 276–295.

Naimie C. E., J. W. Loder and D. R. Lynch (1994) Seasonal variation of the three-dimensional residual circulation on Georges Bank. *Journal of Geophysical Research*, **99**(C8), 15,967–15,989.

Nihoul J. C. J., editor (1980) *Marine Turbulence*, Elsevier, p. 378.

Nihoul J. C. J., E. Deleersnijder and S. Djenidi (1989) Modelling the general circulation of shelf seas by 3D $k-\varepsilon$ models. *Earth Science Reviews*, **26**, 163–189.

Nihoul J. C. J. and B. M. Jamart, editors (1987) *Three-dimensional models of marine and estuarine dynamics*, Elsevier, p. 629.

Okubo A. (1971) Oceanic diffusion diagrams. *Deep-Sea Research*, **18**, 789–802.

Pacanowski R. C. and S. G. H. Philander (1981) Parameterization of vertical mixing in numerical models of tropical oceans. *Journal of Physical Oceanography*, **11**, 1443–1451.

Panofsky H. A. (1963) Determination of stress from wind and temperature measurements. *Quarterly Journal of the Royal Meteorological Society*, (89), 85–94.

Rodi W. (1984) *Turbulence models and their application in hydraulics—a state of the art review*. International Association for Hydraulics Research, 2nd edition, p. 104.

Røed L. P. and C. K. Cooper (1987) A study of various open boundary conditions for wind-forced barotropic numerical ocean models. In: *Three-dimensional models of marine and estuarine dynamics*, J. C. J. Nihoul and B. Jamart, editors, Elsevier, pp. 305–336.

Ruddick K. G., E. Deleersnijder, T. De Mulder and P. Luyten (1994) A model study of the Rhine discharge front and downwelling circulation. *Tellus*, **46A**, 149–159.

Sharples J. and J. H. Simpson (1995) Semi-diurnal and longer period stability cycles in the Liverpool Bay region of freshwater influence. *Continental Shelf Research*, **15**(2/3), 295–313.

Simpson J. H., W. G. Bos, F. Schirmer, A. J. Souza, T. P. Rippeth, S. E. Jones and D. Hydes (1993) Periodic stratification in the Rhine ROFI in the North Sea. *Oceanologica Acta*, **16**(1), 23–32.

Simpson J. H. and A. J. Souza (1995) Semi-diurnal switching of stratification in the Rhine ROFI. *Journal of Geophysical Research*, **100**(c4), 7037–7044.

Smith S. D. and E. G. Banke (1975) Variation of the sea surface drag coefficient with wind speed. *Quarterly Journal of the Royal Meteorological Society*, **101**, 665–673.

Stern M. E., J. A. Whitehead and B. L. Hua (1982) The intrusion of a density current along the coast of a rotating fluid. *Journal of Fluid Mechanics*, **123**, 237–265.

van Alphen J. S. L. J., W. P. M. de Ruijter and J. C. Borst (1988) Outflow and three-dimensional spreading of Rhine river water in the Netherlands coastal zone. In: *Physical processes in estuaries*, J. Dronkers and W. van Leussen, editors, Springer-Verlag, pp. 70–92.

van der Giessen A., W. P. M. de Ruijter and J. C. Borst (1990) Three-dimensional current structure in the Dutch coastal zone. *Netherlands Journal of Sea Research*, **1/2**(25), 45–55.

Visser A. W., A. J. Souza, K. Hessner and J. H. Simpson (1994) The effect of stratification on tidal current profiles in a region of freshwater influence. *Oceanologica Acta*, **17**(4), 369–381.

Weatherly G. L. and P. J. Martin (1978) On the structure and dynamics of the oceanic bottom boundary layer. *Journal of Physical Oceanography*, **8**(4), 557–570.

Zimmerman J. T. F. (1986) The tidal whirlpool: A review of horizontal dispersion by tidal and residual currents. *Netherlands Journal of Sea Research*, **2/3**(20), 133–154.

APPENDIX A

Stratification for a sheared water column

An idea of the sensitivity of stratification to the diffusion coefficient can be achieved by considering a simplified problem with the plume as a surface layer of constant thickness D slipping with velocity u_{res} over a bottom layer with constant salinity S_0. Denoting salinity in the surface layer as $S(s,z)$, where s is the distance from the river mouth along a residual streamline, neglecting the products of tidal fluctuations, and supposing a constant diffusion coefficient, λ_0, the governing equation for tidally-averaged salinity along a residual streamline reduces to:

$$u_{res}\frac{\partial S}{\partial s}=\frac{\partial}{\partial z}\left(\lambda_0\frac{\partial S}{\partial z}\right) \tag{A.1}$$

subject to the boundary condition at the river mouth (A.2), the sea surface (A.3) and the surface-bottom layer interface (A.4):

$$S|_{s=0}=S_0+(S_1-S_0)\left(\cos\frac{\pi z}{2D}\right) \tag{A.2}$$

$$\left.\frac{\partial S}{\partial z}\right|_{z=0}=0 \tag{A.3}$$

$$S|_{z=-D}=S_0. \tag{A.4}$$

This set of equations has solution:

$$S(s,z)=S_0+(S_1-S_0)\left(\cos\frac{\pi z}{2D}\right)e^{-(\lambda_0\pi^2 s)/(4D^2u_{res})} \tag{A.5}$$

and the bottom-top salinity difference is given by:

$$\Delta S(s)=S(s,-D)-S(s,0)=\Delta S(0)e^{-(\lambda_0\pi^2 s)/(4D^2u_{res})} \tag{A.6}$$

implying an exponential, dependence of far-field stratification on the diffusion coefficient, λ_0. This model is obviously a gross simplification of processes in reality, since both u_{res}, D and S_0 depend also on λ_0, and cannot be considered constant in space. Moreover tidal-averaging introduces the products of fluctuations, which contribute also to the salinity budget, but have been neglected here. However, the strong dependence of ΔS on λ_0 suggested by this model is inescapable.

APPENDIX B

How important is advection of turbulence?

The importance of advection of k compared to, say, dissipation can be assessed by an order of magnitude analysis of the relevant terms:

$$X = \frac{\text{Advection}}{\text{Dissipation}} = \frac{|\nabla_h(\mathbf{u}k)|}{\left|\frac{2^{3/2}k^{3/2}}{B_1 l}\right|} \sim \frac{\mathcal{U}}{\mathcal{L}_x}\frac{B_1 l}{2^{3/2}\sqrt{k}} \tag{B.1}$$

where $\mathcal{U}$ is a typical velocity, and $\mathcal{L}_x$ is a horizontal length scale characteristic of variations of $\mathbf{u}$ or k. Now taking $\mathcal{U} < 1\ \mathrm{m\ s^{-1}}$ and $\mathcal{L}_x \geq \Delta x = 10^3\ \mathrm{m}$ for the domain considered and using the constraint (18), an upper limit, $X_{\max}$ can be calculated for X:

$$X \leq X_{\max} = \frac{1\ \mathrm{m\ s^{-1}}}{10^3\ \mathrm{m}}\frac{16.6}{2^{3/2}}\sqrt{\frac{0.56}{N^2}} = \frac{4.4 * 10^{-3}\mathrm{s^{-1}}}{N}. \tag{B.2}$$

Taking even a (for this region) weak stratification of 1 psu over 10 m gives $N^2 = 7.5 * 10^{-4}\ \mathrm{s^{-2}}$ and $X_{\max} = 0.16 \ll 1$, and we can conclude that horizontal (and vertical) advection of k can be neglected. The analysis of the importance of advection of turbulence in the case where the water column is vertically well-mixed and horizontal gradients are strong is beyond the scope of the present analysis, though it has been studied by Deleersnijder (1992).